A new hydroxyanthraquinone derivative with a low and reversible capacity fading process as negolyte in alkaline aqueous redox flow batteries

S. Guiheneuf, T. Godet-Bar, J.-M. Fontmorin, C. Jourdin, D. Floner, Florence Geneste

A new hydroxyanthraquinone derivative with a low and reversible capacity fading process as negolyte in alkaline aqueous redox flow batteries

S. Guiheneuf,[a] T. Godet-Bar,[b] J-M. Fontmorin,[a] C. Jourdin,[a] D. Floner,[a] F. Geneste[a]

[a] Univ Rennes, CNRS, ISCR, UMR 6226, F-35000 Rennes, France

[b] Kemiwatt, 11 allée de Beaulieu CS 50837 F-35708 Rennes Cedex 7

Corresponding author:

Dr Solène Guihéneuf (E-mail address: solene.guiheneuf@univ-rennes1.fr)

Highlights:

- 2,3-DHAQ is a new and promising negolyte for AORFB
- This aqueous RFB exhibits high energy efficiency and good cycling stability
- A 3000 cycles experiment was reported
- The observed capacity fading was reversible by modifying discharge parameters

Graphical abstract:

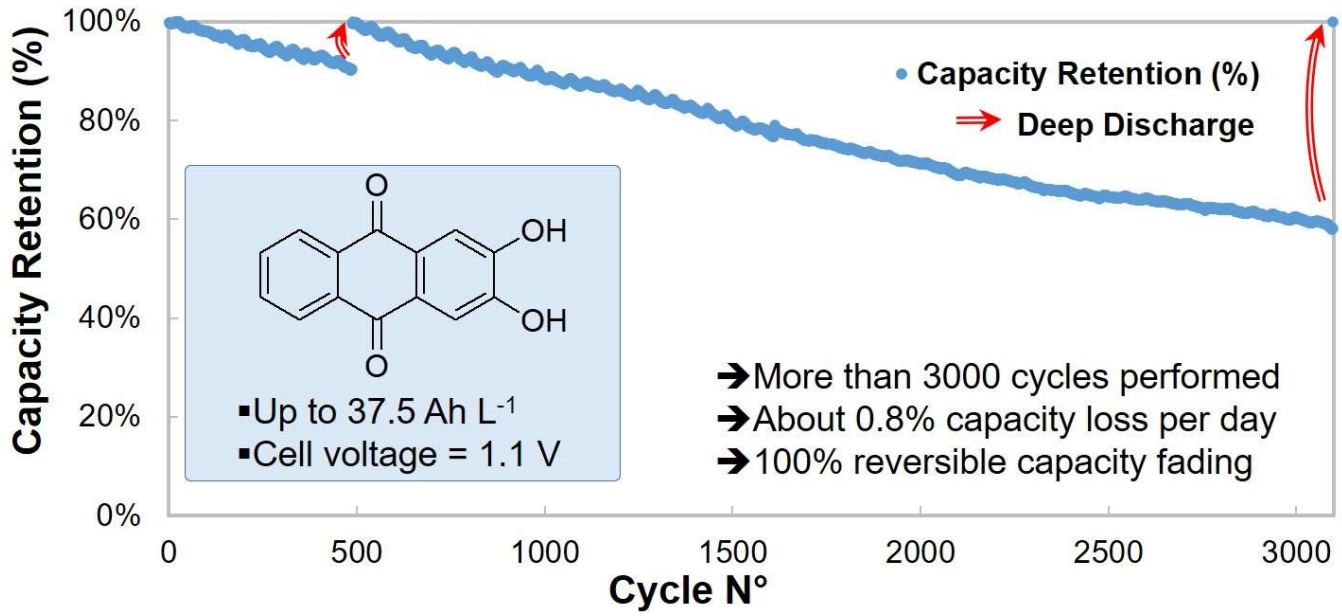

Abstract:

2,3-dihydroxylated anthraquinone (2,3-DHAQ) is evaluated for the first time in a redox flow battery. This compound exhibits a good solubility in alkaline media (0.7 M in KOH at pH > 13.5) and a suitable potential (-0.85 V *vs* Ag/AgCl) leading to a 1.11 V theoretical open circuit voltage at 50% state of charge with potassium ferrocyanide as posolyte. It is implemented in a 25 cm² cell during 180 cycles with a capacity fading of 0.022% per cycle and a current efficiency higher than 99.7%. Owing to its high solubility, an initial energy density up to 17 Wh L^{-1} (7.7 Wh L^{-1} when both posolyte and negolyte are considered) is obtained. 2,3-DHAQ exhibits a good chemical stability compared with other dihydroxyanthraquinone (around 0.1% per cycle). After more than 3000 cycles, 2,3-DHAQ is observed as the main product, showing its high chemical stability. Moreover, the capacity fading process is reversible since changing the discharge conditions allows a full recovery of the initial capacity. This opens up new perspectives as the capacity loss is often used to evaluate the relevance of new molecules. A wider range of active materials in AORFB can be considered if the capacity fading they exhibit can be reversible.

Keywords: Renewable energy; Aqueous organic redox flow battery; Dihydroxyanthraquinone; Long lifetime battery; Electrolyte

1. Introduction

The storage of renewable energies is one of the prime challenges for the future in order to reduce the carbon footprint and improve the management of resources (intermittence of energies supplies as solar and wind, peak demands…). In this context, redox flow batteries are a very promising technology. Indeed, the supplied power and the energy density can be independently tuned by a proper material and chemical design. In the prospect of a more sustainable exploitation of ores, organic material as electroactive molecules are a widely explored alternative as they are earth abundant and could lead to less expensive systems [1–6].

Many organic compounds have been described as negolyte for aqueous redox flow battery (AORFB) [7–10]. Among these scaffolds, anthraquinones, which have been reported regarding various electrochemical storage systems [11], have been selected as good candidates for negolyte in AORFB. They are reduced in a two-electron reversible or quasi-reversible process and their properties in terms of solubility and potential can be easily adapted by slight modifications of their structure [7,12]. Anthraquinone derivatives were

reported as negolyte at various pH. In acidic conditions, the 2,7-AQDS/Bromine AORFB exhibited an open circuit potential (OCV) of 0.8 V at 50% state of charge (SoC) and a discharge capacity retention of 99.8% per cycle over 750 cycles [13,14]. In order to reduce corrosion due to drastic acidic media, pH closer to neutral was considered. For example, the 2,7-AQDS/Iodine AORFB reached an OCV of ~1 V and a 98% current efficiency although its long-term stability was not studied [15]. For the purpose of increasing the cell voltage, dissymmetric pH conditions were also explored as the 2,7-AQDS (pH 8)/Bromine (pH 2) AORFB, leading to a 1.3 V OCV over 200 cycles [16,17]. Alkaline media offer the advantage of being less corrosive than the acidic ones and allow the deprotonation of many functional groups such as phenol leading to a wider range of water-soluble compounds. Furthermore, at high pH, the redox process of some anthraquinone derivatives does not involve proton transfer, hence advantageously, the potential does not change with pH fluctuation during the redox process [12]. In alkaline conditions, dihydroxyanthraquinones (DHAQs) are particularly interesting and are represented by several commercially available isomers with different solubility, cost and electrochemical stability. Anthraflavic acid (2,6-DHAQ) is the most studied among DHAQs since its first use as negolyte has been reported in an aqueous alkaline medium [18]. 2,6-DHAQ was also described in hybrid acid and base system to gain higher cell voltage and energy density but such strategy requires a close monitoring and regular adjustment of the electrolytes pH [19]. Further work has been performed on the evaluation of 2,6-DHAQ in alkaline media regarding its chemical stability; the formation of anthrone and its dimer derivative from a disproportionation – oxidative coupling side reaction has been reported during the battery charge [4,20–22]. In a previous study we also reported the role of the counter ion on the solubility of 3,4-dihydroxy-9,10-anthraquinone-2-sulfonic acid (ARS) [23]. An energy density up to 20 Wh L^{-1} was reached in AORFB with the potassium salt of ARS, more than twice higher than the sodium salt, with a capacity fading of 0.03% per cycle. An electrochemically reversible degradation product (3-hydroxy-9,10-anthraquinone-2-sulfonic acid HAQS) resulting from a hydrodeoxygenation reaction was identified and synthesized to be tested in AORFB. Interestingly, this new anthraquinone exhibited a lower capacity fading of 0.012% per cycle (0.29% per day) [23]. In order to improve their solubility, DHAQs were also functionalized with solubilizing chains. For example, alizarin-3-methyliminodiacetic acid (AMA) exhibited a solubility of 0.4 M and led to a high stability with less than 0.02% of capacity fading per cycle [24]. Another approach is the alkylation of the OH groups by solubilizing chains [25–27]. Capacity fadings below 0.5% per day have been reported with these alkylated DHAQs with operating pH ranging from 7 to 13 [28]. The solubility of DHAQs depends on the

position of the hydroxyl groups on the aromatic ring. Thus, commercial DHAQs with OH groups in positions 1, 4, 5 and/or 8 have low solubilities (below 0.15 M) in aqueous alkaline media. Chen *et al.* were able to improve the solubility of 1,8-DHAQ from 0.08 M to 3 M in KOH by adding choline hydroxide as a hydrotropic agent. Although this approach is interesting, a higher viscosity led to capacity fading and the adsorption of choline chloride on the electrode inhibited the electrochemical kinetic of 1,8-DHAQ [29]. Table 1 summarized results concerning commercial DHAQ as negolytes in alkaline medium with $K_4Fe(CN)_6$ as posolyte, which is to this date the more common molecule described as posolyte in literature for alkaline AORFB [18,23,24,27,30–40].

DHAQ	**Cycles**	**Capacity fading per cycle (day)**	**CE (%)**	**EE (%)**	**Max power density (mW cm^{-2}); ASR (ohm cm²)**	**References**
2,6-DHAQ[a]	100	0.1% (8%)	>99	84	450; 0.88	[18]
AMA[a]	350	0.02% (0.81%)	~100	84.9	490; 0.81	[24]
ARSNa[b]	100	0.35% (4.4%)	~100	83	182; 2.4	[23]
1,8-DHAQ[c]	100	0.12% (13%)	99.3	77	111; 2.5	[29]
2,3-DHAQ[b]	**180**	**0.022% (0.45%)**	**>99.7**	**84.3**	**189; 2.2**	**This work**

Table 1 Cycle number, capacity fading, CE, EE, maximal power density and area specific resistance (ASR) of described DHAQs. a: current density 100 mA cm^{-2}; b: current density 40 mA cm^{-2}; c: current density 80 mA cm^{-2}.

2,3-DHAQ can be obtained by organic synthesis [41,42] or by extraction from *Streptomycesgalbus* [43]. To our knowledge, this compound known for its properties as dye [44] and therapeutic applications [41,45], has never been evaluated as negolyte in alkaline AORFBs, although it has been previously reported that hydroxyl groups in position 2, 3, 6 and/or 7 increase the solubility in alkaline medium and also allow a lower standard potential [7,12]. In this work, the solubility and electrochemical behavior of 2,3-DHAQ were first studied. As expected, with its two hydroxyl groups in position 2 and 3, this molecule exhibited a high solubility and a suitable potential to reach an OCV higher than 1 V. Although the solubility and electrochemical behavior of DHAQs has been previously reported [12,29], 2,3-DHAQ has never been studied in AORFBs. We selected 2,3-DHAQ as a new target since it can be obtained in a one-step synthesis making it one of the cheapest dihydroxyanthraquinone with high solubility and a suitable potential for AORFB application. In addition to

highlighting a new redox compound particularly attractive for AORFB application, our results contribute to increase the knowledge regarding DHAQs properties and behavior. Furthermore, when evaluated in alkaline aqueous redox flow batteries, 2,3-DHAQ exhibited one of the lowest capacity fading rate compared with other DHAQs [18,28,29], although it is important to note that cycling conditions are different for every compounds since no standard cycling procedure are used in AORFB evaluations. The cycling conditions as the applied current density or the cut-off voltage have a tremendous influence on capacity fade rates as it will be demonstrated in this work. A 3000-cycle experiment also displayed a good capacity retention and the full recovery of the initial capacity when a more negative discharge potential was used, confirming that 2,3-DHAQ is a relevant candidate for electrolyte engineering. The reversibility of the capacity fading process is a key parameter as it could increase drastically the lifetime of the battery.

2. Experimental

2.1 Procedure and materials for synthesis and analysis

All reagents were used without further purification. Sodium chloride (99%+) was purchased from Sigma-Aldrich (USA), aluminum chloride (98.5%), catechol (99%+) and phthalic anhydride (99%) were purchased from Acros (Belgium). Concentrated hydrogen chloride (35%), potassium hydroxide (85%), sodium hydroxide (98%), potassium ferrocyanide hexahydrate (96%) and ethanol (99.5%) were purchased from VWR (US). D_2O and DMSO-d_6 was purchased from Euriso-top (France). ^{1}H NMR spectra were recorded on BRUKER AC 300 P (300 MHz) spectrometer and ^{13}C NMR spectra on BRUKER AC 300 P (75 MHz) spectrometer. Chemical shifts are expressed in parts per million using the deuterated solvent as a reference. Data are given in the following order: value, multiplicity (s, singlet; d, doublet; t, triplet; q, quadruplet; m, multiplet; br, broad), number of protons, coupling constants *J* is given in Hertz. The mass spectra were realized on a Waters Q-Tof 2 and elemental analysis was performed on a Thermo Fisher Flash 1112 at the Centre Régional de Mesures Physiques de l'Ouest (CRMPO, Rennes). UV-Visible measurements were carried out on an Agilent Technologies Cary 60 using a Scan software. The cycling management was performed with the BT-Lab V1-57 software controlling a BioLogic Science Instruments BCS 815. pH values were measured with a Mettler Toledo SG23-ELK Seven Go Duo pH/cond with 3 calibration values (4, 7 and 10).

2.2 Organic synthesis

As a typical example, 2,3-DHAQ was prepared based on a modified procedure from Zhang *et al.* [41]. Sodium chloride (9 g, 154 mmol, 5.7 eq) was prebaked at 110°C and then aluminum chloride (40 g, 300 mmol, 11.1 eq) was added. The mixture was heated at 120°C in an oil bath until melting. Phthalic anhydride (4 g, 27 mmol, 1 eq) and catechol (2.98 g, 27 mmol, 1 eq) were grinded together in a ceramic mortar. The homogeneous powder obtained was added by portion on the molten mixture of $AlCl_3$/NaCl. The reaction was performed at 145°C for 23 h. After returning to room temperature, 100 mL of 10% aqueous hydrogen chloride (prepared from concentrated hydrogen chloride and ultrapure water) was added to disperse the black crude along with 150 mL of ultrapure water. The resulting suspension was heated in an oil bath at 110°C for 2 h then brought to room temperature. After a filtration on a Buchner, the precipitate was washed with 30 mL 10% aqueous HCl then with 40 mL hot ethanol. The product was isolated after drying under vacuum (10^{-2} mbar at 40°C for 8 h). A 82:18 ratio of 2,3-DHAQ/1,2-DHAQ mixture was obtained as a dark green powder (yield 2,3-DHAQ 44%; yield 1,2-DHAQ 10%; purities 2,3-DHAQ 78%/1,2-DHAQ 17% determined by internal standard ^{1}H NMR).

2,3-DHAQ (78% purity) ^{1}H NMR (300 MHz, DMSO-d_6) δ 10.76 (s, 2H), 8.13 (dd, *J* = 5.7, 3.3 Hz, 2H), 7.85 (dd, *J* = 5.7, 3.3 Hz, 2H), 7.59 (s, 2H). ^{13}C NMR (75 MHz, DMSO-d_6) δ 182.11, 152.15, 134.38, 133.69, 127.25, 126.83, 113.52. 1,2-DHAQ (17% purity)^{1}H NMR (300 MHz, DMSO) δ 12.59 (s, 1H), 10.83 (s, 1H), 8.24 – 8.09 (m, 2H), 7.96 – 7.83 (m, 2H), 7.64 (d, *J* = 8.3 Hz, 1H), 7.22 (d, *J* = 8.3 Hz, 1H). MS ESI (EI-) $[M-H]^-$ (C_{14} H_7 O_4) theoretical: 239.03498; found: 239.0350. Elemental analysis: 67.18% C (70.00% theoretical); 3.35% H (3.36% theoretical).

2.3 Solubility measurements

A calibration curve was performed using solutions from 10^{-5} to 10^{-4} M concentrations. The 2,3-DHAQ solubility was determined by UV-Vis in 1.2 M aqueous potassium hydroxide in triplicate. First, 100 mg of 2,3-DHAQ (purity 78% of 2,3-DHAQ and 17% of 1,2-DHAQ) was mixed with the tested solvent by 100 µL portions until no solid remains. A more accurate value was obtained with an UV-Vis titration on the diluted (1/10000^e) solution isolated after filtration (0.22 µm filter) of saturated samples after 24 h, 48 h and 72 h at 40°C and a 24 h delay to return to 20°C and stabilize. The solubility was also measured at various pH at 25°C by adding

portions of an 8 M KOH aqueous solution under stirring on a 2,3-DHAQ suspension (ratio of 93:7 of 2,3-DHAQ/1,2-DHAQ) until the targeted pH was reached and stable. At each targeted pH, 200 µL of the suspension were collected, filtered on 0.22 µm filters and analyzed by UV-visible spectrometry to obtain the concentration. For the maximum solubility measurement of the reduced form, a 100% charge of a 0.35 M solution of 2,3-DHAQ (ratio of 93:7 of 2,3-DHAQ/1,2-DHAQ) was realized and the electrolyte was filtered (0.22 µm filter) in a glovebox. Then UV-Visible analysis was performed (both initial and final solutions were diluted by 10 000 in KOH 1 M).

2.4 Electrochemical measurements

The electrochemical experiments were conducted on an electrochemical working station (BioLogic Science Instruments VSP) using a three-electrode electrochemical cell, where a Pt wire was employed at the counter electrode (CE), an Ag/AgCl/KCl saturated electrode immerged in a 1M KOH solution protected from the cell solution by a porous glass frit served as the reference electrode (RE) and a rotating disc electrode (RDE) mounted with a glassy carbon (GC, 7.069 mm²) disk was used as the working electrode (WE). The potential was reported relative to the Ag/AgCl reference electrode. Ohmic drop compensation was performed on the basis of the value of the resistance of the solution between the WE and RE, which was determined by current-interrupt experiments. Before each electrochemical measurement, the GC disk electrode was polished using SiC P4000 foil.

Each recorded cyclic voltammetry of the reduction and the oxidation process of a compound at a given scan rate was analyzed by measuring $i_{p,a}$ = anodic peak current; $i_{p,c}$ = cathodic peak current; v = scan rate; $E_{p,a}$ = anodic peak potential; $E_{p,c}$ = cathodic peak potential; $\Delta E_p = E_{p,a}-E_{p,c}$; the apparent standard redox potential $E^{0'} = (E_{p,a}+E_{p,c})/2$.

The oxidant diffusion coefficient D ($cm^2\ s^{-1}$) was calculated using the Randles-Sevcik equation $i_p = 0.4463.n.F.A.C.(n.F.v.D/(R.T)^{-})^{1/2}$, n = number of electron exchanged during the redox process; F = Faraday constant = 96485 C mol^{-1}; A = electrode active area (cm^2); C = redox active molecule concentration (mol cm^{-3}); R = gas constant = 8.314 J K^{-1} mol^{-1}; T = bulk temperature = 293 K; v = scan rate (V s^{-1}). The diffusion-limited current was plotted against the square root of rotation speed (Figure S1) and a correlation coefficient close to 100% was obtained from the regression straight line, confirming that the peak current is proportional

to the square root of the scan rate and that the redox process is diffusion controlled. The diffusion coefficient was calculated from the slope of the regression straight line.

The apparent heterogeneous rate constant k^0 was calculated using the Koutecký-Levich equation $1/I = 1/i_K + 1/(0.62.n.F.A.D_O^{2/3}.\omega^{1/2}.\upsilon^{-1/6}.C)$ [46]; i_K represents the kinetic current observed in the absence of any mass-transfer limitations (extrapolation to infinite rotation rate); ω represents the angular rotation rate of the RDE (rad s^{-1}); υ is the kinematic viscosity of the solution (cm^2 s^{-1}); F is the Faraday constant = 96485 C mol^{-1}; A is the electrode active area (cm^2); C is the redox active molecule concentration (mol cm^{-3}); n is the number of electrons exchanged during the redox process. The experiments were conducted with an RDE by linear sweep voltammetry (LSV) at various rotation speeds ranging from 400 rpm to 2500 rpm. The current (i) at various applied overvoltage (η) from $E_{1/2}$ value (between 10 and 80 mV overvoltage with 10 mV increments) was plotted against the reciprocal of the square root of the angular rotation rate ($\omega^{-1/2}$), giving rise to the i_K values. A plot of $\eta = \log(i_K)$ (Figure S2) was linearly fitted to the Tafel plot ($\eta = [2.3.R.T/\alpha.F]\log(i_0) - [2.3.R.T/\alpha.F]\log(i_K)$) at the overpotential of zero to deduce the exchange current density (i_0) (Figure S3), from which the k^0 value was determined according to the Butler-Volmer equation ($i_0 = n.F.A.C.k^{0'}$).

Pourbaix diagrams of 10^{-3} M 1,2-DHAQ (alizarin) and 10^{-3} M 2,3-DHAQ were carried out in 0.1 M carbonate buffer ($Na_2CO_3/NaHCO_3$) and a concentrated KOH solution to cover a 9 to 14 pH range. pH of the buffered solutions was adjusted stepwise with a concentrated KOH solution or with concentrated HCl (Figure S4).

2.5 Cell experiments

RFB experiments were carried out with a BCS-815 battery cycler (Biologic) at room temperature in a home-made cell with graphite felt electrodes (SGL carbon SE; square cuboid 50 × 50 × 4.6 mm with a geometrical surface area of 25 cm^2; 35% compression of the thickness leading to 95.5% porosity), composite graphite current collectors and cationic ion-exchange membrane (Aquivion® E98-08 Solvay 80 µm Nafion 117 membrane). Felts and membrane were used as received. The positive and negative electrolytes were pumped at a flow rate of 150 mL min^{-1} (180 cycles experiment) and 350 mL min^{-1} (3000 cycles experiment) through KNF Pump (Liquiport® 1.100 version KT). The battery was operated through a BT-Lab V1-57 software controlling a BioLogic Science Instruments BCS 815. Electrolytes were typically prepared as following: negolyte was a 50 mL solution of 0.3 M 2,3-DHAQ in aqueous KOH (1.8 M) and posolyte was a 60 mL solution of 0.5 M potassium ferrocyanide in aqueous NaOH (0.2 M).

3. Results and discussion

3.1 Synthesis of 2,3-DHAQ

Although the synthesis of 2,3-DHAQ has been previously described in literature [47–50], the pure compound could not be isolated on a gram scale. The best results were obtained with the procedure reported by Zhang *et al.* with phthalic anhydride and catechol in melted $AlCl_3$/NaCl [41]. Following this synthetic procedure, NMR analysis revealed a mixture of 1,2-DHAQ and 2,3-DHAQ with 2,3-DHAQ as the main product (80-95%) as previously reported by Pozzo *et al.* [42]. To improve the regioselectivity of the reaction towards the formation of 2,3-DHAQ, the effect of temperature (from 130°C to 160°C), reaction time (from 4 h to 48 h) and hydrogen chloride solution (concentration, amount and temperature during the addition) was investigated but it did not have a drastic influence on the regioselectivity of the reaction. The 2,3-DHAQ/1,2-DHAQ ratio was slightly increased with a larger amount of $AlCl_3$/NaCl eutectic salt and by increasing the volume of aqueous HCl used at the end of the reaction. However, we decided to keep a lower amount of $AlCl_3$/NaCl to decrease aluminum containing effluents [42]. Furthermore, since the reaction medium was highly viscous, temperature higher than 135°C, vigorous stirring and increased reaction time were used. The separation of 2,3-DHAQ and 1,2-DHAQ could be performed at a small scale by sublimation or by a derivatization - crystallization sequence [42] but as we needed higher amounts for our experiments and as the 1,2-DHAQ isomer is also electroactive and soluble up to 0.19 M in 1 M KOH, we did not investigate further purification process. Finally, we obtained a mixture of 2,3-DHAQ and 1,2-DHAQ in 44% and 10% yields, respectively. The purity was determined by NMR with an internal standard (78% for 2,3-DHAQ and 17% for 1,2-DHAQ) and was in good accordance with the elemental analysis (96% from the carbon analysis for the mixture of DHAQs). This simplified synthetic procedure avoided material loss during the purification process and was more adapted to AORFB application. Further purifications steps by column chromatography leading to 2,3-DHAQ with a 2,3/1,2-DHAQ ratio of 93:7 were performed for solubility measurement *vs* pH and electrochemical analysis.

3.2 Solubility and half-wave potential

The solubility of 2,3-DHAQ measured by the shake-flask method was found to be 0.6 M in 1.2 M KOH at 20°C and 0.7 M in 2 M KOH, which corresponds to a theoretical capacity of 37.5 Ah L^{-1}. The solubility of 2,3-

DHAQ was compared to other hydroxyanthraquinones at pH 14 (Table 2). Previous reports stated that the hydroxyl position on the aromatic ring is a critical parameter influencing the solubility and the electrochemical standard potential [7,12,51–53]. Thus, OH groups on positions 2, 3, 6 and 7 led to higher solubilities whereas on positions 1, 4, 5 and 8, they have a detrimental effect on solubility. This is confirmed by the high solubility found for 2,3-DHAQ (0.7 M), which is similar to 2,6-DHAQ. A comparable tendency is noticeable concerning the standard potential since hydroxyl groups on positions 2, 3, 6 and 7 induce a shift to more negative potentials (Table 2) as it has been previously reported by Cao *et al.* [12,29].

Positions	Solubility (M)	Potential (V vs Ag/AgCl)	References
1,2	0.19	-0.85	[12]
1,4	0.15-0.11[a]	-0.74	[12]
1,5	0.15-0.13[a]	-0.75	[12]
1,8	0.08	-0.77	[12]
2,3	**0.7**	**-0.85**	**This work**
2,6	>0.6	-0.91	[12]

Table 1 Solubilities of DHAQs at pH 14 in KOH. [a] thixotropic behavior.

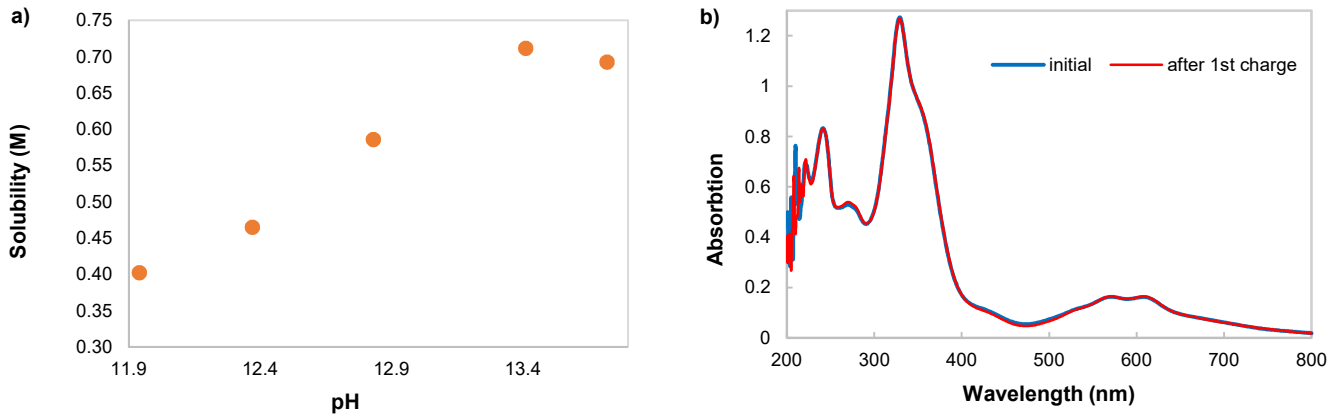

Figure 1 a) Solubility *vs* pH in aqueous KOH solutions at 25°C; b) UV-visible absorption spectra of a 0.35 M solution of 2,3-DHAQ in KOH 1.8 M before and after a 100% charge (spectra recorded on an aerated sample).

The solubility of 2,3-DHAQ *vs* pH was measured by UV-Visible spectrophotometry from pH 11.9 to 13.7 (Figure 1a). The solubility increased with the pH and reached a concentration of 0.5 M (1 M electrons) for pH > 12.5 and 0.7 M (1.4 M electrons) for pH > 13.5. This value is more than three times higher than the solubility

reported for its isomer 1,2-DHAQ (i.e. 0.19 M in KOH 1 M [29]). We also evaluated the solubility of the reduced form by charging a 0.35 M solution of 1,2-DHAQ at 100% SoC. The value of the initial concentration of anthraquinone was chosen slightly higher than the concentration used for the redox flow battery experiment to ensure that the limit of solubility could not be reached during the charge-discharge processes. The electrolyte was filtered in a glovebox and a UV-Visible spectrophotometry analysis was performed on the aerated sample. No difference was observed between the spectra of 2,3-DHAQ and the spectra after a 100% charge, filtration and oxidation at air (Figure 1b), showing that the solubility of the reduced electrolyte was at least 0.35 M in aqueous KOH.

The redox process reversibility evaluation was conducted at diluted state (Figures S5 to S6 and Table S1), on a 6.3 mM solution at pH 14 buffered with 1 M of KOH, on a batch of synthesized 2,3-DHAQ comprising 87% of DHAQ isomers (93:7 ratio of 2,3-DHAQ/1,2-DHAQ). 2,3-DHAQ exhibited a quasi-reversible wave at -0.85 V *vs* Ag/AgCl. As depicted in Table 3, the difference between anodic and cathodic peak potentials (ΔE_p) was around 90 mV, significantly higher than the value for 1,2-DHAQ (ΔE_p close to 31-37 mV) but close to the ΔE_p of 2,6-DHAQ. It has been previously reported by Cao *et al.* that the position of the hydroxyl groups on the anthraquinone backbone plays an important role in the reversibility and the charge transfer fastness of the redox system. For example, 1,5-DHAQ redox system was less reversible than the 1,8-DHAQ one with a ΔE_p of 201 mV and 32 mV, respectively [29]. These ΔE_p discrepancies were correlated by the authors to the stability of the intermediate anionic radical brought by its high number of resonance structures, leading to more important electron delocalization [29]. Another hypothesis would be that the redox process is a bit slowed down by a conformation rearrangement [32]. It has also been reported that a single two-electron fully reversible wave is observed for quinones in aqueous medium, whereas two waves are visible in anhydrous aprotic medium, due to the high stabilization of the quinone dianion by a strong hydrogen-bonding with water molecules [54,55]. Furthermore, intramolecular hydrogen bonds in α-phenolic quinones significantly contributes to the stabilization of the reduced quinone species [56]. Such strong intramolecular hydrogen bonding interactions could explain the lower ΔE_p values of 1-hydroxyanthraquinones, although further investigations would be necessary to confirm this hypothesis.

Overall, taking into account all reversibility criteria, the reduction process of the compound involved two electrons as it will be confirmed by the initial experimental capacity obtained in RFB and is said reversible and fast.

The diffusion coefficient of 3.4 x 10^{-6} cm² s^{-1} was measured by linear sweep voltammetry on a rotating disk electrode and calculated from the Randles-Sevcik equation. The electron transfer rate constant k^0 was estimated from the Koutecký-Levich equation, providing a 1.56 x 10^{-2} cm s^{-1} value. The same electrochemical characterization of 1,2-DHAQ was performed and the diffusion coefficient and the standard rate constant were similar to previously reported values (i.e. k^0: 1.7 x 10^{-2} cm s^{-1} and D: 4.5 x 10^{-6} cm² s^{-1}), indicating that the position of the hydroxyl groups has a low influence on the electrochemical constants (Table 3). The potential of 2,3-DHAQ allowed a theoretical OCV at 50% SoC of 1.11 V (Figure 2a). This value was similar to other DHAQ isomers, except for 2,6-DHAQ which exhibits a slightly higher OCV of 1.2 V (Table 3). The electrochemical behavior of 2,3-DHAQ was also studied at positive potentials by cyclic voltammetry (Figure 2b). The compound was irreversibly oxidized at 0.15 V and 0.37 V, leading to the apparition of two new systems at -0.26 V and -0.49 V, getting more intense after several cycles. This behavior seems to be related to the formation of $(DHA)_2$ as it has been previously described with 2,6-DHAQ by Goulet *et al.* [22].

DHAQ	ΔE (mV)	k^0 (cm s^{-1})	D (cm² s^{-1})	TheoreticaOCV SoC 50% (V)	References
2,6	95	7.0 x 10^{-3} Oldham	4.8 x 10^{-6} Levich	1.2	[18]
AMA	-	8.4 x 10^{-3} Koutecký-Levich	6.7 x 10^{-6} Levich	1.23	[24]
ARSNa	49	1.2 × 10^{-3} Tafel plot	6.2 × 10^{-7} Levich	1.25	[23]
1,2	40	4.3 x 10^{-2} Koutecký-Levich	5.1 x 10^{-6} Randles-Sevcik	1.1	[29]
1,8	32	1.7 x 10^{-2} Koutecký-Levich	8.4 x 10^{-6} Randles-Sevcik	1.1	[29]
2,3	**88**	**1.56 x 10^{-2} Koutecký-Levich**	**3.4 x 10^{-6} Randles Sevcik**	**1.11**	**This work**

Table 2 Electron transfer rate constant and diffusion coefficient of described DHAQs.

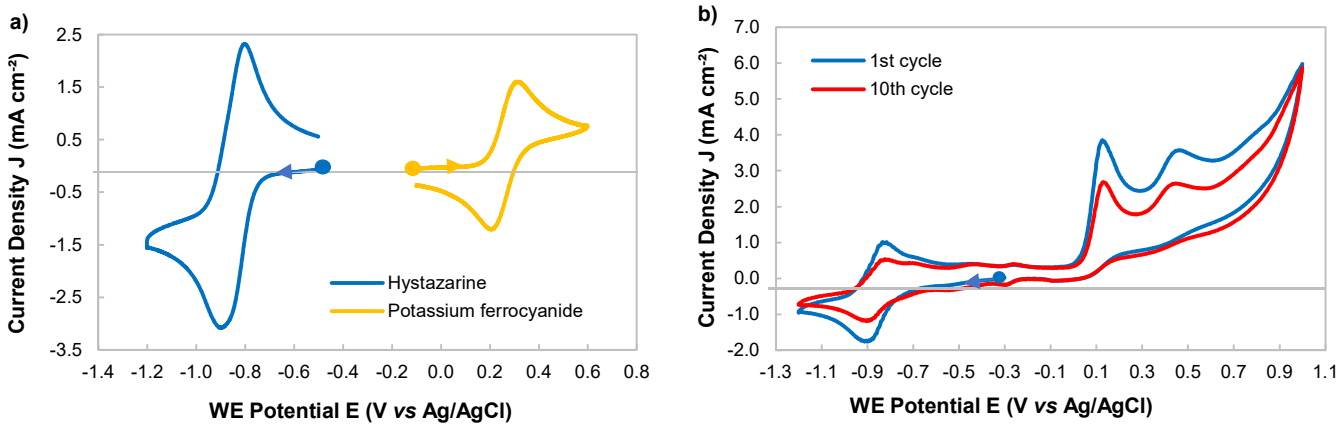

Figure 2 a) Cyclic voltammograms on glassy carbon electrode of 10mM solutions of 2,3-DHAQ and $K_4Fe(CN)_6$ in aqueous KOH at pH 14, 100 mV s^{-1}; b) Cyclic voltammograms on glassy carbon electrode of 1mM solutions of 2,3-DHAQ.

In order to better assess the suitability of 2,3-DHAQ for RFB applications, the evolution of the apparent half-wave potential ($E_{1/2,app}$) *vs* pH was studied. Considering that 2,3-DHAQ used for the analysis contains 1,2-DHAQ, the behavior of 2,3-DHAQ was compared to that of a solution of 1,2-DHAQ. The pH was limited to the range in which 2,3-DHAQ was soluble (i.e. 10^{-3} M for pH ≥ 9). As depicted in Figure 3a, the Pourbaix diagram ($E_{1/2,app}$ *vs* pH) of 2,3-DHAQ can be fitted to two lines of slopes -50.0 mV pH^{-1} (9.34 ≤ pH ≤ 12.02) and 0.0 mV pH^{-1} (12.52 ≤ pH ≤ 14.00). The second slope of 0.0 mV pH^{-1} corresponds to a $2e^-/0$ proton process whereas the first slope of -50.0 mV pH^{-1} can reasonably be attributed to a $2e^-/2$ protons process (theoretically -59.0 mV pH^{-1}). The difference between the slope measured and the theoretical value can be explained by comparing the Pourbaix diagram of 2,3-DHAQ to that of the 1,2-DHAQ solution. As can be seen in Figure 3b, the Pourbaix diagram of 1,2-DHAQ can be fitted to two lines of slopes -34.4 mV pH-1 (9.24 ≤ pH ≤ 12.21) and 0.0 mV pH^{-1} (12.42 ≤ pH ≤ 14.00), suggesting a $2e^-/1$ proton process followed by a $2e^-/0$ proton process. Despite the close structures of 2,3-DHAQ and 1,2-DHAQ, it was reported that the position of the hydroxyl groups on the anthraquinones has a significant impact on their pKa value(s) and electrochemical behaviours [29]. Therefore, the slope of -50 mV pH^{-1} (instead of the theoretical value of -60 mV for a $2e^-/2$ protons process) for 2,3-DHAQ can likely be explained by the contribution of the 1,2-DHAQ to the 2,3-DHAQ signal. Although quinones typically undergo three successive redox processes as the pH increases ($2e^-$/2protons, $2e^-/1$ proton and $2e^-/0$ proton), the $2e^-/1$ proton process theoretically corresponding to a slope of 30 mV could not be observed for 2,3-DHAQ. It can be assumed that the absence of the $2e^-/1$ proton process is due to very close pKa values that make the 30 mV slope indiscernible. Similar behaviours were reported in literature, for example with 2,6-DHAQ that followed a $2e^-/2$ protons process at 10 ≤ pH ≤ 12 (-61 mV pH^{-1} slope) directly

followed by a $2e^-/0$ proton process at pH > 12 (0 mV pH^{-1} slope) [18]. Based on the Pourbaix diagram described above, 2,3-DHAQ is thus a good negolyte candidate for RFBs as it can reach a potential of -0.85V *vs* Ag/AgCl at pH ≥ 12.

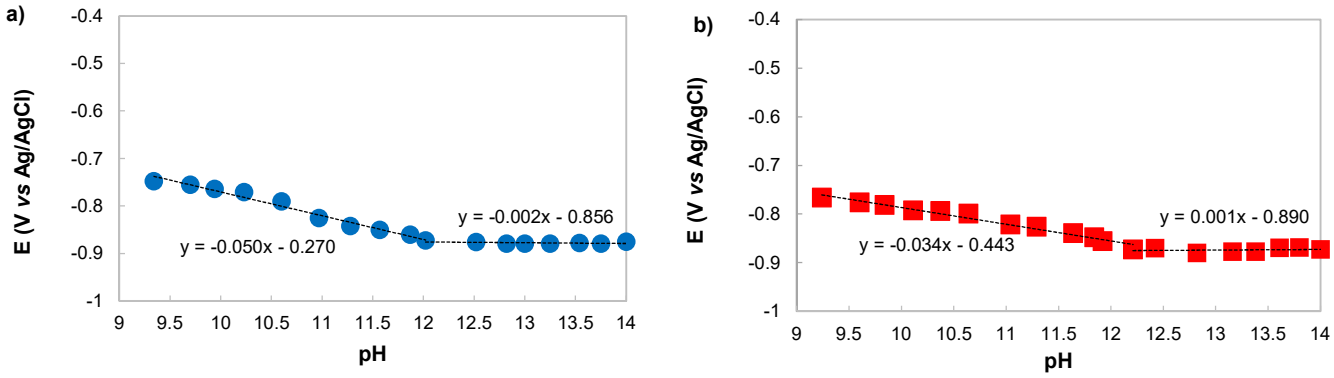

Figure 3 Pourbaix diagrams of a) 2,3-DHAQ (containing 1,2-DHAQ) and b) 1,2-DHAQ.

3.3 Flow battery experiment

3.3.1 Preliminary evaluation with 180 cycles

This experiment was conducted on a 0.3 M 2,3-DHAQ solution in 1.8M KOH containing 45 mM 1,2-DHAQ formed during the synthesis. The cycling current density was set at 40 mA cm^{-2} both in charge and discharge and voltage cut-offs were set at 0.7 and 1.5 V (Figure 4a). The capacity decreased to 96% of the initial capacity after 180 cycles, indicating a capacity fading of 0.022% per cycle (0.45% per day). This value is lower than the capacity fading reported for other DHAQs (Table 1) [18,24,29]. This result demonstrates the influence of the position of the functional groups on the aromatic ring since the stability seems to be higher when there is no hydroxyl group on position 1. At a current density of 40 mA cm^{-2}, the coulombic efficiency was higher than 99.7% (Figure 4b), showing that the molecule was relatively stable and that no crossover from negolyte to posolyte occurred. The initial energy density was 17 Wh L^{-1} and slightly decreased to 16.3 Wh L^{-1} (7.7 Wh L^{-1} and 7.4 Wh L^{-1}, respectively considering volumes of both negolyte and posolyte) (Figure 4b). The energy efficiency around 84.3% was quite stable and the voltage efficiency reached 84.5% after 180 cycles (Figure 4c). These results are similar to energy and voltage efficiencies previously reported with other DHAQs (Table 1). The resistance increased by almost 21% from 1.84 to 2.23 ohm cm^2 over the 180

cycles (Figure 4d). Since the global resistance is mainly governed by the membrane and the interfacial resistance [57], the gain of resistance could result from a pollution of the membrane by the electrolytes or from a decline of the electron transfer kinetic. The OCV at 50% SoC was measured at 1.18 V (Figure 4d). The maximal power density reached 189 mW cm^{-2} which is lower than values reported for 2,6-DHAQ but higher than 1,8-DHAQ (Table 1). This is explained by the higher resistance (> 2 Ohm cm^2) in the system. It is worth noting that resistance and power are in a large proportion governed by the cell design and materials. Indeed, the flow distribution (e.g., interdigitated gaskets, pumping technology and flow rate), the membrane thickness and pre-treatment and the electrode pretreatment can lead to significant gaps when comparing results obtained from different cell designs. In this work the 80 µm Nafion membrane and the SGL graphite felts were used without pre-treatment, explaining the higher resistance, hence lower power measured compared to 2,6-DHAQ and AMA.

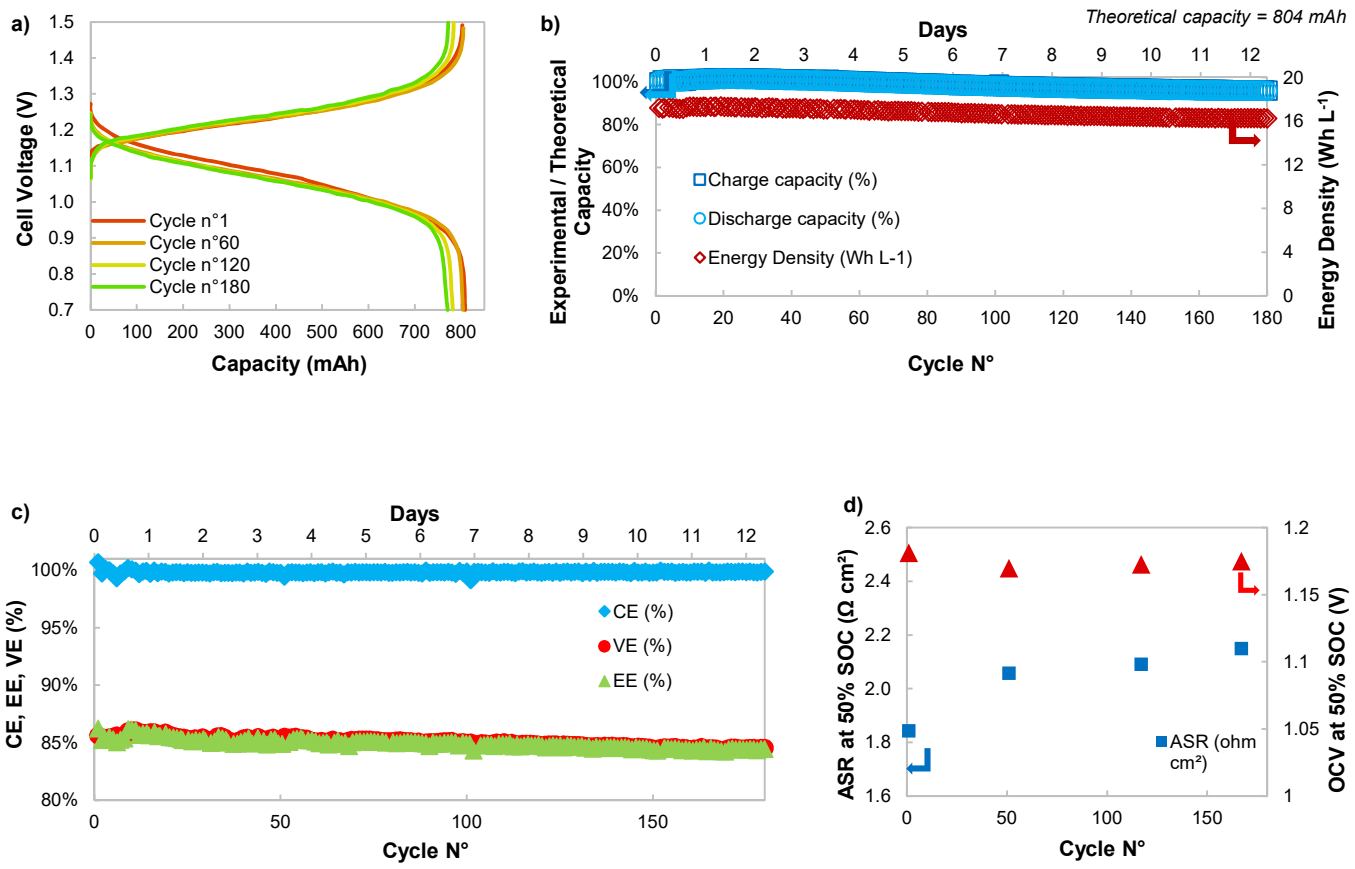

Figure 4 a) Potential *vs* capacity curves for cycle 1, 60, 120 and 180; b) Charge and discharge capacity (% *vs* theoretical capacity) and Energy density of the negolyte *vs* cycle number; c) CE, VE and EE (%) *vs* cycle number; d) ASR and OCV *vs* cycle number. Electrolytes were prepared as following: negolyte was a 50 mL solution of 0.3 M 2,3-DHAQ in aqueous KOH 1.8 M; posolyte was a 60 mL solution of 0.5 M potassium ferrocyanide in aqueous NaOH (0.2 M).

After cycling, cyclic voltammetry analysis of the negolyte (Figure 5a) showed that the signature of the electrolyte was close to the initial system with however a wider ΔE_p value (~160 mV). It can be attributed to a decrease of conductivity due to supporting salt migration threw the membrane during the charge-discharge process, an apparent increase of viscosity and/or a slower kinetic (loss of reversibility). UV-visible spectra (Figure 5b) of the diluted solution before and after cycling were compared and no significant change was observed. The concentration of negolyte after cycling was estimated by ^{1}H NMR with an internal standard (Figure 5c), showing no degradation of 2,3-DHAQ. The presence of 2,3-DHAQ was not observed in the posolyte (Figure 5d and S6), showing that no crossover of the anthraquinone through the membrane occurred. Although it was not observed in ^{1}H NMR, MS analysis showed traces of $(DHA)_2$. The formation of $(DHA)_2$ was previously reported by Goulet *et al.* [22] with 2,6-DHAQ used as negolyte. Indeed, low potential anthraquinones are sensitive to a disproportionation - dimerization process making DHAQs especially vulnerable. Furthermore, this reaction could be favored by the high cut-off voltage of 1.5 V applied in charge. Regardless, the capacity retention of 96% after 180 cycles proved that this degradation process occurred in a small amount. Since it has been reported that the increase of the pH decreases anthrone production [35], the high concentration of hydroxide in the electrolyte would limit this side-reaction.

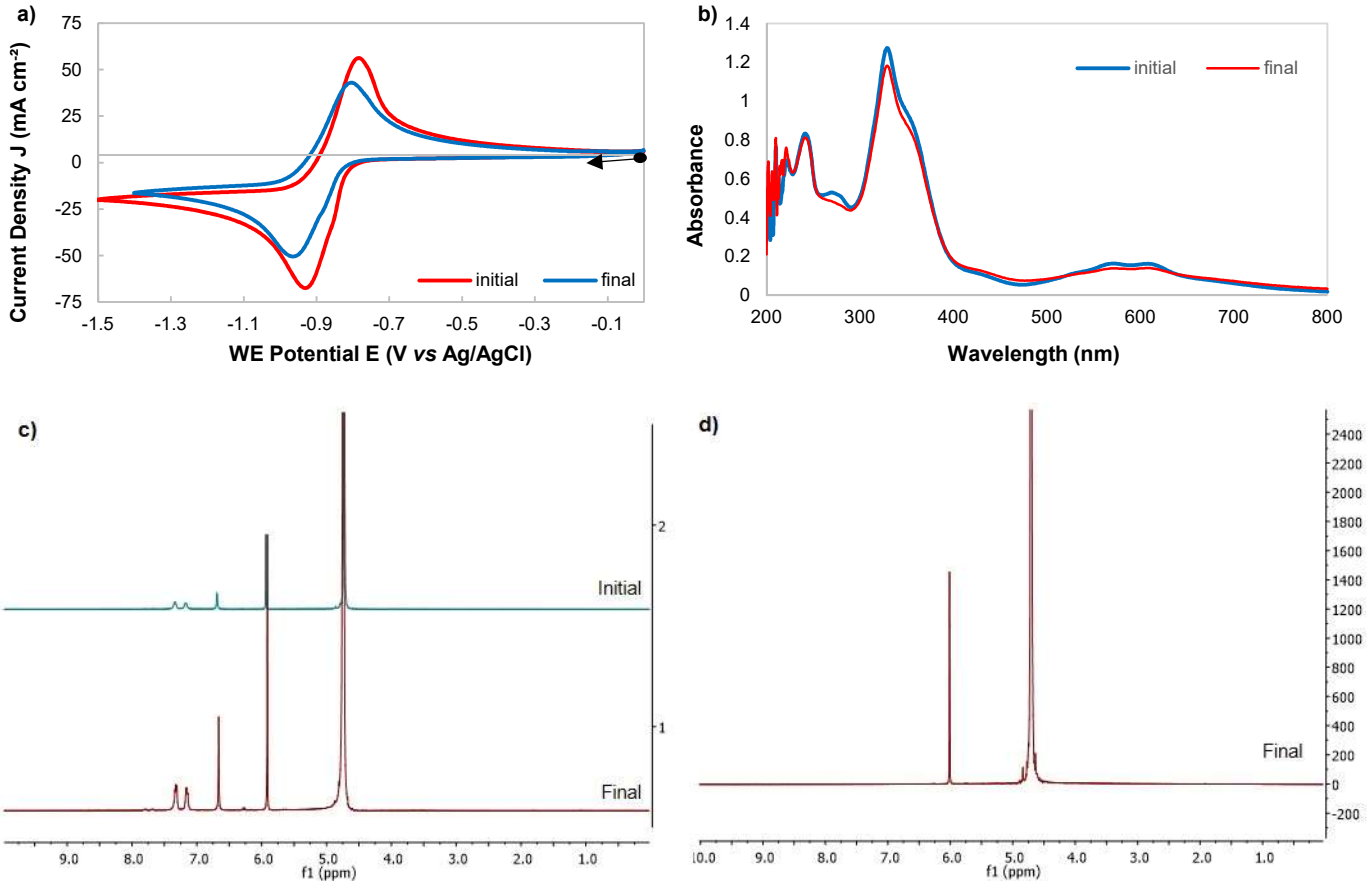

Figure 5 a) cyclic voltammetry of the negolyte before (red) after (blue) cycling (glassy carbon) 100 mV s^{-1}; b) UV-visible spectra of the negolyte diluted by KOH 1M before (red) and after (blue) 180 cycles; c) ^{1}H NMR with internal standard (maleic acid 5.92 ppm) of the negolyte before (red) and after (blue) 180 cycles; d) ^{1}H NMR with internal standard (maleic acid 5.92 ppm) of the posolyte after 180 cycles.

3.3.2 Long term cycling evaluation of 3000 cycles

A long-term experiment was conducted over the course of two months for a more accurate evaluation of 2,3-DHAQ stability. A lower cut-off voltage of 1.3V was applied in charge to limit the formation of $(DHA)_2$ and the capacity loss was compensated by a constant voltage step at 1.3 V with a 50 mA current limit (CV step) [22,58]. A CV step at 0.85 V was also applied in discharge with a 50 mA current limit.

The OCV was measured at different SoC, from 10 to 100%. At 50% SoC, the value was 1.13 V in good accordance with the theoretical value calculated from cyclic voltammetry and reached 1.23 V at 90% SoC (Figure 6a). The ASR increased at SoC below 20% and above 80% (Figure 6a). Considering the important flow rate that was used during this cell test, the mass transport polarization is neglected. The polarization ASR measurement is consistent with standard AORFB behavior [27] where most of the measured resistance is capacitive and is coming from the membrane and where a minor contribution of this ASR is faradaic and is coming from the charge transfer polarization of both redox molecules. This charge transfer polarization is lower at mid SoC (equilibrium between oxidized and reduced forms) and higher when lowering or increasing the SoC where a depletion of each redox specie form (oxidized or reduced) occurs.

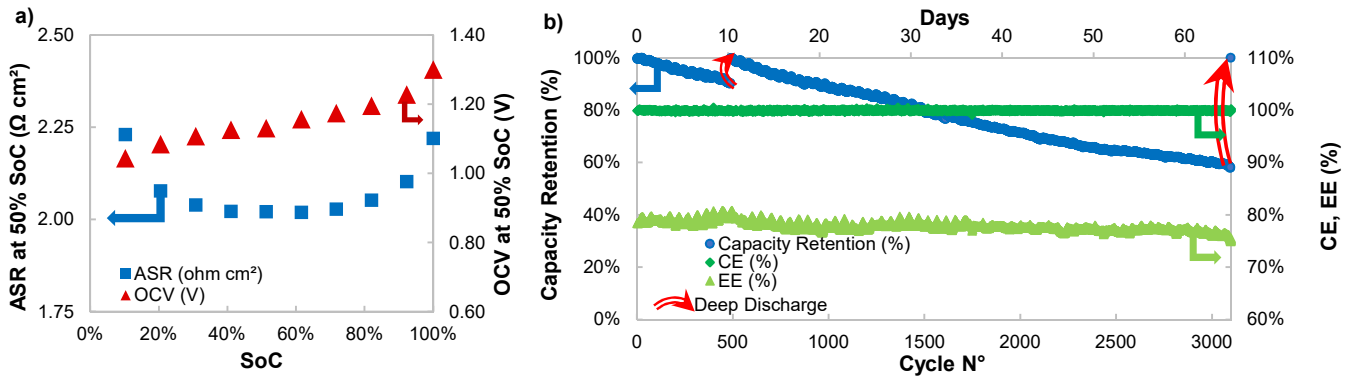

Figure 6 a) ASR and OCV and *vs* number of cycles; b) CE, EE and capacity retention *vs* number of cycles. Electrolytes were prepared as following: negolyte was a 40 mL solution of 0.2 M 2,3-DHAQ in aqueous KOH 1.8 M; posolyte was a 44 mL solution of 0.5 M potassium ferrocyanide in aqueous NaOH (0.2 M).

During the first 600 cycles, a capacity fading of -0.019% per cycle was obtained (Figure 6b), in the same order of magnitude than the previous experiment. After 600 cycles, a deep discharge was performed at 1 A with a cut-off voltage of 0.4 V and all the lost capacity was regained, showing that the capacity fading process was reversible. A similar capacity fading rate, -0.016% per cycle (i.e., -0.8% per day), was observed for the cycling process from 600 to 3 000 cycles. This result underlines the good stability compared to other described systems, especially considering the high cycle number. Indeed, most described experiments regarding DHAQs report less than 1000 cycles [18,24,28,29]. At the end of the experiment, 100% of the initial capacity was regained with a new deep discharge at lower current density (100 mA) with a cut-off voltage of 0.5 V, indicating that no irreversible chemical transformation of the molecule took place. We hypothesized that the formation of the anthrone dimer took place during the experiment, leading to a capacity fading as the formed dimer is not electroactive. However, the oxidation performed during the deep discharge induced the recovery of the initial 2,3-DHAQ compound and of its corresponding capacity. This hypothesis was recently confirmed by the work of Jing *et al.* [59].

In order to assess how the battery performance evolves while increasing current densities, a specific cycling test was carried out. Ten different current densities were applied, ranging from 30 to 100 mA cm^{-2}, four cycles were recorded for each current density. In order to avoid secondary reactions (e.g. water electrolysis), a reduced voltage range of 0.85 V-1.3 V was chosen and constant voltage steps were added at the upper voltage limit during charge process (1.3 V) and at the lower voltage limit during discharge process (0.85 V), both CV steps were stopped at a current limit of 50 mA. The fourth cycle of each tested current density was represented in Figure 7a. The evolution of the coulombic (CE) and energy (EE) efficiencies along with the current densities were plotted in Figure 7c. The coulombic efficiency (CE) ranged between 99.8% and 100% and slightly increased with the current densities. The energy efficiency (EE) evolved linearly with the current density, decreasing from 89.8% at 30 mA cm^{-2} down to 75.0% at 100 mA cm^{-2}. Since mass transport and charge transfer (electron transfer kinetics) polarizations are considered to be negligible in this battery test, the decrease of EE with the current density is mainly due to ohmic resistance.

Considering the capacity retention calculated after each current density loops of four cycles, the capacity loss slightly increased with the current density (Figure 7e), from 0.1% per day at 30 mA cm^{-2} to 0.6% per day at 50 and 70 mA cm^{-2}. This led us to think that the observed capacity fading was not only a calendar phenomenon but was also correlated to the duration of the CV step at 1.3 V performed at the end of each

charge, which increased along with the current density. This result tends to show that the 2,3-DHAQ degradation kinetic increases as it is longer subjected to more negative potential, as previously observed [59].

A second cycling study was also performed to assess the battery performance evolution in closer conditions than the ones that are used in a real battery application. In this case, constant power mode was used instead of galvanostatic mode with similar cut-off voltages (0.85-1.3 V) and with a CV step during the charge only. Ten different power densities were applied, ranging from 25.5 mW cm^{-2} (which means that a current density of 30 mA cm^{-2} is reached at 0.85 V) up to 85 mW cm^{-2}. Four cycles were recorded for each power densities and the fourth one of each tested power density was plotted in Figure 7b. The evolution of the coulombic (CE) and energy (EE) efficiencies along with the current densities are plotted in Figure 7d. The coulombic efficiency (CE) ranged between 99.8% and 100%. The energy efficiency (EE) evolved linearly with the current density, decreasing from 92.4% at 25.5 mW cm^{-2} down to 80.1% at 85 mW cm^{-2}.

The fast electron transfer kinetics of both redox-active materials allows the energy efficiency of the battery to remain very satisfying (80%), even at relatively high power densities (85 mW cm^{-2}). In addition, we can speculate that decreasing the membrane thickness would improve the battery performances as long as other features like membrane mechanical failure or redox-active material cross-contamination do not appear.

Considering the capacity retention (Figure 7f), we can observe that the majority of the initial discharge capacity is still available when increasing the power density. Indeed, increasing the power density from 25.5 up to 85 mW cm^{-2} only decreases the capacity by 6.7%. The linearity between capacity retention and power density demonstrates that the battery electrochemical process is mainly influenced by ohmic phenomena, which confirms the very good electrochemical performances of the 2,3-DHAQ/ferrocyanide AORFB.

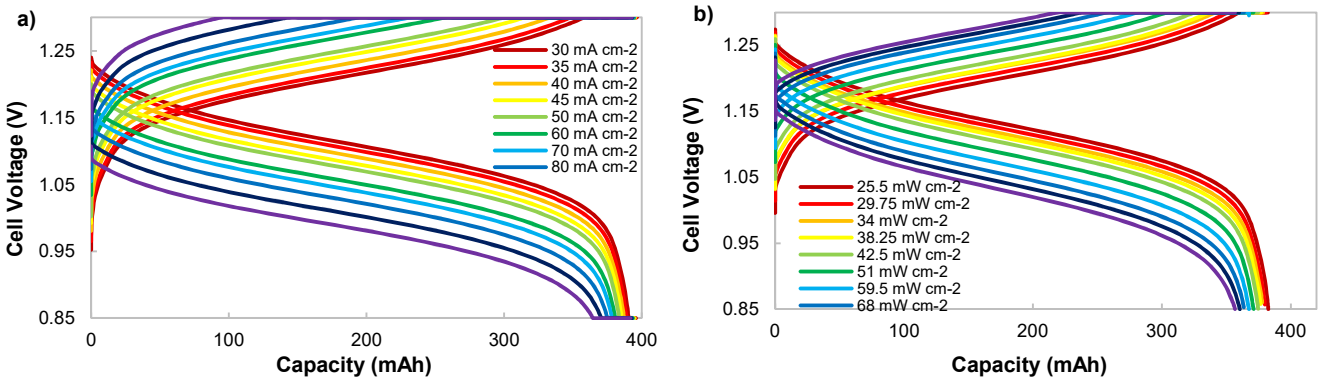

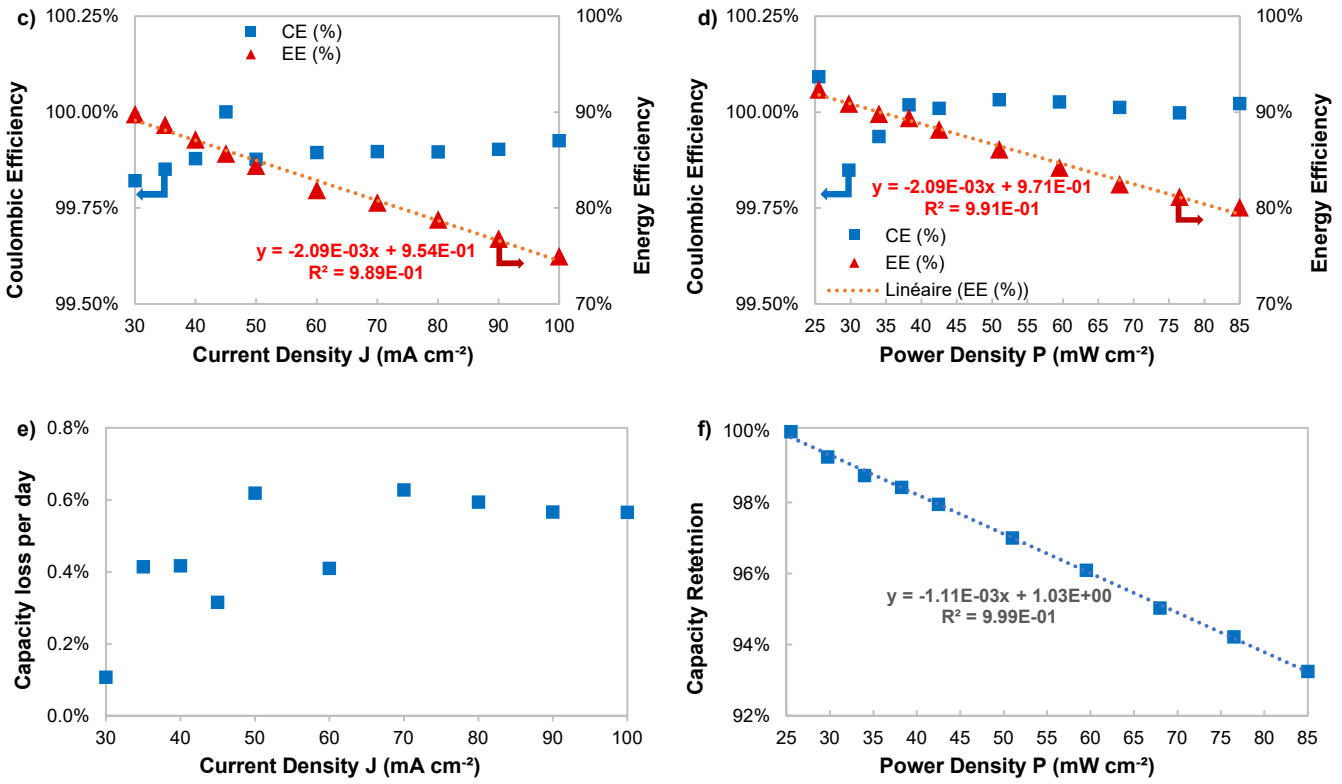

Figure 7 a) Cell voltage *vs* capacity of the 4th cycle at each tested current density; b) Cell voltage *vs* capacity of the 4th cycle at each tested power density; c) CE and EE *vs* current density recorded for the 4th cycle at each current densities; d) CE and EE *vs* density recorded for the 4th cycle at each power density; e) Capacity loss (%) *vs* current density after 4 cycles at each current density; f) Capacity retention (%) *vs* power density after 4 cycles at each power density. Electrolytes were prepared as following: negolyte was a 40 mL solution of 0.2 M 2,3-DHAQ in 1.8 M aqueous KOH; posolyte was a 44 mL solution of 0.5 M potassium ferrocyanide in aqueous NaOH (0.2 M).

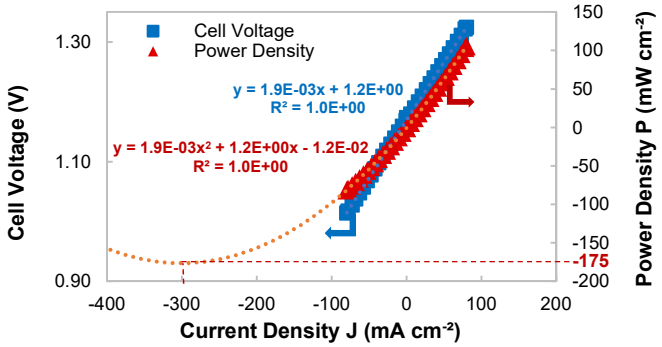

Figure 8 Cell Voltage (blue squares) and Power Density (red triangles) *vs* Current Density at 50% SoC.

During the cycling test, the ASR slightly increased from 1.93 ohm cm² to 2.14 ohm cm² and the maximum power density was relatively stable around 170 mW cm^{-2}. A typical polarization curve is reported in Figure 8. These values are close to those obtained after the 180 cycles experiment and demonstrate that no process

inducing a higher resistance (membrane pollution, drastic increase of the viscosity…) occurred despite the much higher cycle number.

2,3-DHAQ analyzed by cyclic voltammetry after cycling (Figure S7) showed a slower kinetic than the initial solution with a ΔE_p value of 390 mV. This could result of a slightly higher viscosity or a loss of conductivity due to salt migration to the posolyte. ^{1}H NMR of the negolyte (Figure S8) showed new organic signals which could be attributed to the degradation of 1,2-DHAQ present in the electrolyte, whereas 2,3-DHAQ was still the main product.

4. Conclusions

In this work, 2,3-DHAQ was used as negolyte in AORFB for the first time. A simplification of the preparation process of the molecule allowed its production at a lab scale with a suitable purity. The presence of 1,2-DHAQ as by-product did not prevent its use in AORFB since the reduction of 1,2-DHAQ is reversible at a potential close to that of 2,3-DHAQ and its solubility reached 0.19 M in basic medium. The electrochemical analyses of the molecule revealed a behavior close to other DHAQs isomers reported in literature (k^0 = 1.56 x 10^{-2} cm s^{-1} and D = 3.4 x 10^{-6} cm^2 s^{-1}). Its maximum solubility (0.7 M at pH 14) allows reaching the energy density required for industrial applications. Preliminary experiments led to promising results with a reversible capacity fading of 0.45% per day over 180 cycles and an energy efficiency of 84.3% with a maximum power density of 189 mW cm^{-2}. A second evaluation over the course of 3000 cycles also led to good performances with a capacity fading of 0.8% per day over 2400 cycles and a maximal power density reaching 170 mW cm^{-2}. The initial capacity could be recovered thanks to a deep discharge indicating that the capacity fading process is not irreversible. Limitations due to the lower solubility of potassium ferrocyanide used as posolyte led to a total energy density of 7.7 Wh L^{-1} but since the solubility of 2,3-DHAQ led to 37.5 Ah L^{-1} charge capacity at pH 14 and about 32 Ah L^{-1} at pH 13, higher performances could be achieved with a more soluble posolyte. This work demonstrates that 2,3-DHAQ could be a good candidate for negolyte engineering owing to its good performances and stability.

5. Acknowledgements

The authors thank la Région Bretagne and BPI France (Concours Mondial de l'Innovation) for financial support. The CRMPO, Centre régional de mesures physiques de l'Ouest realized the mass spectrometry analysis.

6. CRediT authorship contribution statement

S. G. Investigation, Visualization, Synthesis, Formal Analysis, Writing –Original Draft, Writing –Review & Editing; T. G.-B. Investigation, Validation, Resources, Writing –Review & Editing, Supervision, Funding Acquisition; J.-M. F. Investigation, Formal Analysis, Visualization, Writing –Review & Editing; C. J. Synthesis, Formal Analysis; D. F. Conceptualization, Validation, Resources, Supervision, Project Administration, Funding Acquisition; F. G. Conceptualization, Validation, Resources, Writing –Review & Editing, Visualization, Supervision, Project Administration, Funding Acquisition.

7. References

[1] J. Luo, B. Hu, M. Hu, Y. Zhao, T.L. Liu, Status and Prospects of Organic Redox Flow Batteries toward Sustainable Energy Storage, ACS Energy Lett. 4 (2019) 2220–2240. https://doi.org/10.1021/acsenergylett.9b01332.

[2] X. Wei, W. Pan, W. Duan, A. Hollas, Z. Yang, B. Li, Z. Nie, J. Liu, D. Reed, W. Wang, V. Sprenkle, Materials and Systems for Organic Redox Flow Batteries: Status and Challenges, ACS Energy Lett. 2 (2017) 2187–2204. https://doi.org/10.1021/acsenergylett.7b00650.

[3] P. Leung, A.A. Shah, L. Sanz, C. Flox, J.R. Morante, Q. Xu, M.R. Mohamed, C. Ponce de León, F.C. Walsh, Recent developments in organic redox flow batteries: A critical review, J. Power Sources. 360 (2017) 243–283. https://doi.org/10.1016/j.jpowsour.2017.05.057.

[4] F.R. Brushett, M.J. Aziz, K.E. Rodby, On Lifetime and Cost of Redox-Active Organics for Aqueous Flow Batteries, ACS Energy Lett. 5 (2020) 879–884. https://doi.org/10.1021/acsenergylett.0c00140.

[5] J. Winsberg, T. Hagemann, T. Janoschka, M.D. Hager, U.S. Schubert, Redox-Flow Batteries: From Metals to Organic Redox-Active Materials, Angew. Chemie - Int. Ed. 56 (2017) 686–711. https://doi.org/10.1002/ange.201604925.

[6] J. Chai, A. Lashgari, J.J. Jiang, Electroactive Materials for Next-Generation Redox Flow Batteries: From Inorganic to Organic, in: ACS Symp. Ser., American Chemical Society, 2020: pp. 1–47.

https://doi.org/10.1021/bk-2020-1364.ch001.

[7] Y. Ding, C. Zhang, L. Zhang, Y. Zhou, G. Yu, Molecular engineering of organic electroactive materials for redox flow batteries, Chem. Soc. Rev. 47 (2018) 69–103. https://doi.org/10.1039/c7cs00569e.

[8] Y. Liu, Q. Chen, P. Sun, Y. Li, Z. Yang, T. Xu, Organic electrolytes for aqueous organic flow batteries, Mater. Today Energy. 20 (2021) 100634. https://doi.org/10.1016/j.mtener.2020.100634.

[9] J. Cao, J. Tian, J. Xu, Y. Wang, Organic Flow Batteries: Recent Progress and Perspectives, Energy and Fuels. 34 (2020) 13384–13411. https://doi.org/10.1021/acs.energyfuels.0c02855.

[10] F. Zhong, M. Yang, M. Ding, C. Jia, Organic Electroactive Molecule-Based Electrolytes for Redox Flow Batteries: Status and Challenges of Molecular Design, Front. Chem. 8 (2020) 451. https://doi.org/10.3389/fchem.2020.00451.

[11] C. Han, H. Li, R. Shi, T. Zhang, J. Tong, J. Li, B. Li, Organic quinones towards advanced electrochemical energy storage: Recent advances and challenges, J. Mater. Chem. A. 7 (2019) 23378–23415. https://doi.org/10.1039/c9ta05252f.

[12] K. Wedege, E. Dražević, D. Konya, A. Bentien, Organic Redox Species in Aqueous Flow Batteries: Redox Potentials, Chemical Stability and Solubility, Sci. Rep. 6 (2016) 39101. https://doi.org/10.1038/srep39101.

[13] Q. Chen, L. Eisenach, M.J. Aziz, Cycling Analysis of a Quinone-Bromide Redox Flow Battery, J. Electrochem. Soc. 163 (2016) A5057–A5063. https://doi.org/10.1149/2.0081601jes.

[14] B. Huskinson, M.P. Marshak, M.R. Gerhardt, M.J. Aziz, Cycling of a Quinone-Bromide Flow Battery for Large-Scale Electrochemical Energy Storage, ECS Trans. 61 (2014) 27–30. https://doi.org/10.1149/06137.0027ecst.

[15] W. Lee, A. Permatasari, B.W. Kwon, Y. Kwon, Performance evaluation of aqueous organic redox flow battery using anthraquinone-2,7-disulfonic acid disodium salt and potassium iodide redox couple, Chem. Eng. J. 358 (2019) 1438–1445. https://doi.org/10.1016/j.cej.2018.10.159.

[16] A. Khataee, K. Wedege, E. Dražević, A. Bentien, Differential pH as a method for increasing cell potential in organic aqueous flow batteries, J. Mater. Chem. A. 5 (2017) 21875–21882. https://doi.org/10.1039/c7ta04975g.

[17] A. Khataee, E. Dražević, J. Catalano, A. Bentien, Performance Optimization of Differential pH Quinone-Bromide Redox Flow Battery, J. Electrochem. Soc. 165 (2018) A3918–A3924.

https://doi.org/10.1149/2.0681816jes.

[18] K. Lin, Q. Chen, M.R. Gerhardt, L. Tong, S.B. Kim, L. Eisenach, A.W. Valle, D. Hardee, R.G. Gordon, M.J. Aziz, M.P. Marshak, Alkaline quinone flow battery, Science (80-.). 349 (2015) 1529–1532. https://doi.org/10.1126/science.aab3033.

[19] M.T. Dizaji, W. Li, Higher voltage redox flow batteries with hybrid acid and base electrolytes, Eng. Sci. 11 (2020) 54–65. https://doi.org/10.30919/es8d1118.

[20] M.-A. Goulet, M.J. Aziz, Flow Battery Molecular Reactant Stability Determined by Symmetric Cell Cycling Methods, J. Electrochem. Soc. 165 (2018) A1466–A1477. https://doi.org/10.1149/2.0891807jes.

[21] D.P. Tabor, R. Gómez-Bombarelli, L. Tong, R.G. Gordon, M.J. Aziz, A. Aspuru-Guzik, Mapping the frontiers of quinone stability in aqueous media: Implications for organic aqueous redox flow batteries, J. Mater. Chem. A. 7 (2019) 12833–12841. https://doi.org/10.1039/c9ta03219c.

[22] M.A. Goulet, L. Tong, D.A. Pollack, D.P. Tabor, S.A. Odom, A. Aspuru-Guzik, E.E. Kwan, R.G. Gordon, M.J. Aziz, Extending the lifetime of organic flow batteries via redox state management, J. Am. Chem. Soc. 141 (2020) 8014–8019. https://doi.org/10.1021/jacs.8b13295.

[23] S. Guiheneuf, A. Lê, T. Godet-Bar, L. Chancelier, J.M. Fontmorin, D. Floner, F. Geneste, Behaviour of 3,4-Dihydroxy-9,10-Anthraquinone-2-Sulfonic Acid in Alkaline Medium: Towards a Long-Cycling Aqueous Organic Redox Flow Battery, ChemElectroChem. 8 (2021) 2526–2533. https://doi.org/10.1002/celc.202100284.

[24] Y. Liu, S. Lu, S. Chen, H. Wang, J. Zhang, Y. Xiang, A Sustainable Redox Flow Battery with Alizarin-Based Aqueous Organic Electrolyte, ACS Appl. Energy Mater. 2 (2019) 2469–2474. https://doi.org/10.1021/acsaem.8b01512.

[25] S. Jin, Y. Jing, D.G. Kwabi, Y. Ji, L. Tong, D. De Porcellinis, M.A. Goulet, D.A. Pollack, R.G. Gordon, M.J. Aziz, A Water-Miscible Quinone Flow Battery with High Volumetric Capacity and Energy Density, ACS Energy Lett. 4 (2019) 1342–1348. https://doi.org/10.1021/acsenergylett.9b00739.

[26] Y. Ji, M.A. Goulet, D.A. Pollack, D.G. Kwabi, S. Jin, D. De Porcellinis, E.F. Kerr, R.G. Gordon, M.J. Aziz, A Phosphonate-Functionalized Quinone Redox Flow Battery at Near-Neutral pH with Record Capacity Retention Rate, Adv. Energy Mater. 9 (2019) 1900039. https://doi.org/10.1002/aenm.201900039.

[27] D.G. Kwabi, K. Lin, Y. Ji, E.F. Kerr, M.A. Goulet, D. De Porcellinis, D.P. Tabor, D.A. Pollack, A. Aspuru-Guzik, R.G. Gordon, M.J. Aziz, Alkaline Quinone Flow Battery with Long Lifetime at pH 12, Joule. 2 (2018) 1894–1906. https://doi.org/10.1016/j.joule.2018.07.005.

[28] D.G. Kwabi, Y. Ji, M.J. Aziz, Electrolyte Lifetime in Aqueous Organic Redox Flow Batteries: A Critical Review, Chem. Rev. 120 (2020) 6467–6489. https://doi.org/10.1021/acs.chemrev.9b00599.

[29] J. Cao, M. Tao, H. Chen, J. Xu, Z. Chen, A highly reversible anthraquinone-based anolyte for alkaline aqueous redox flow batteries, J. Power Sources. 386 (2018) 40–46. https://doi.org/10.1016/j.jpowsour.2018.03.041.

[30] C. Wang, X. Li, B. Yu, Y. Wang, Z. Yang, H. Wang, H. Lin, J. Ma, G. Li, Z. Jin, Molecular Design of Fused-Ring Phenazine Derivatives for Long-Cycling Alkaline Redox Flow Batteries, ACS Energy Lett. (2020) 411–417. https://doi.org/10.1021/acsenergylett.9b02676.

[31] D.R. Chang, Y. Kim, S. Jung, Comprehensive study of the performance of alkaline organic redox flow batteries as large-scale energy storage systems, Int. J. Energy Res. 43 (2019) 4449–4458. https://doi.org/10.1002/er.4573.

[32] A. Orita, M.G. Verde, M. Sakai, Y.S. Meng, A biomimetic redox flow battery based on flavin mononucleotide, Nat. Commun. 7 (2016) 13230. https://doi.org/10.1038/ncomms13230.

[33] J. Rodriguez, C. Niemet, L.D. Pozzo, Fluorenone Based Anolyte for an Aqueous Organic Redox-Flow Battery, ECS Trans. 89 (2019) 49–59. https://doi.org/10.1149/08901.0049ecst.

[34] X. Zu, L. Zhang, Y. Qian, C. Zhang, G. Yu, Molecular Engineering of Azobenzene-Based Anolytes Towards High-Capacity Aqueous Redox Flow Batteries, Angew. Chemie - Int. Ed. 59 (2020) 22163–22170. https://doi.org/10.1002/anie.202009279.

[35] M. Wu, Y. Jing, A.A. Wong, E.M. Fell, S. Jin, Z. Tang, R.G. Gordon, M.J. Aziz, Extremely Stable Anthraquinone Negolytes Synthesized from Common Precursors, Chem. 6 (2020) 1432–1442. https://doi.org/10.1016/j.chempr.2020.03.021.

[36] L. Tong, M.A. Goulet, D.P. Tabor, E.F. Kerr, D. De Porcellinis, E.M. Fell, A. Aspuru-Guzik, R.G. Gordon, M.J. Aziz, Molecular Engineering of an Alkaline Naphthoquinone Flow Battery, ACS Energy Lett. 4 (2019) 1880–1887. https://doi.org/10.1021/acsenergylett.9b01321.

[37] C. Wang, Z. Yang, Y. Wang, P. Zhao, W. Yan, G. Zhu, L. Ma, B. Yu, L. Wang, G. Li, J. Liu, Z. Jin, High-Performance Alkaline Organic Redox Flow Batteries Based on 2-Hydroxy-3-carboxy-1,4-

naphthoquinone, ACS Energy Lett. 3 (2018) 2404–2409. https://doi.org/10.1021/acsenergylett.8b01296.

[38] W. Lee, G. Park, Y. Kwon, Alkaline aqueous organic redox flow batteries of high energy and power densities using mixed naphthoquinone derivatives, Chem. Eng. J. 386 (2020) 123985. https://doi.org/10.1016/j.cej.2019.123985.

[39] Z. Yang, L. Tong, D.P. Tabor, E.S. Beh, M.A. Goulet, D. De Porcellinis, A. Aspuru-Guzik, R.G. Gordon, M.J. Aziz, Alkaline Benzoquinone Aqueous Flow Battery for Large-Scale Storage of Electrical Energy, Adv. Energy Mater. 8 (2018) 1702056. https://doi.org/10.1002/aenm.201702056.

[40] A. Hollas, X. Wei, V. Murugesan, Z. Nie, B. Li, D. Reed, J. Liu, V. Sprenkle, W. Wang, A biomimetic high-capacity phenazine-based anolyte for aqueous organic redox flow batteries, Nat. Energy. 3 (2018) 508–514. https://doi.org/10.1038/s41560-018-0167-3.

[41] Z. Zhang, X. Li, T. Song, Y. Zhao, Y. Feng, An Anthraquinone Scaffold for Putative, Two-Face Bim BH3 α-Helix Mimic, J. Med. Chem. 55 (2012) 10735–10741. https://doi.org/10.1021/jm301504b.

[42] J.-L. Pozzo, G.M. Clavier, M. Colomes, H. Bouas-Laurent, Different synthetic routes towards efficient organogelators: 2,3-substituted anthracenes, Tetrahedron. 53 (1997) 6377–6390. https://doi.org/10.1016/S0040-4020(97)00297-4.

[43] C. Balachandran, Y. Arun, V. Duraipandiyan, S. Ignacimuthu, K. Balakrishna, N.A. Al-Dhabi, Antimicrobial and Cytotoxicity Properties of 2,3-Dihydroxy-9,10-Anthraquinone Isolated from Streptomyces galbus (ERINLG-127), Appl. Biochem. Biotechnol. 172 (2014) 3513–3528. https://doi.org/10.1007/s12010-014-0783-8.

[44] O. Otłowska, M. Ślebioda, M. Wachowiak, M. Śliwka-Kaszyńska, A multi-analytical approach to the characterization of natural organic dyestuffs and inorganic substrates present in the 19th-century artistic oil paints manufactured by a French art materials supplier Richard Ainès, Anal. Methods. 9 (2017) 94–102. https://doi.org/10.1039/c6ay02959k.

[45] C. Balachandran, N. Emi, Y. Arun, N. Yamamoto, P.T. Perumal, In vitro antiproliferative activity of 2,3-dihydroxy-9,10-anthraquinone induced apoptosis against COLO320 cells through cytochrome c release caspase mediated pathway with PI3K/AKT and COX-2 inhibition, Chem. Biol. Interact. 249 (2016) 23–35. https://doi.org/10.1016/j.cbi.2016.02.016.

[46] S. Treimer, A. Tang, D.C. Johnson, A consideration of the application of Koutecký-Levich plots in the

diagnoses of charge-transfer mechanisms at rotated disk electrodes, Electroanalysis. 14 (2002) 165–171. https://doi.org/10.1002/1521-4109(200202)14:3<165::AID-ELAN165>3.0.CO;2-6.

[47] N. Hossein, N. Roozberh, Facile, Efficient and One-Pot Synthesis of Anthraquinone Derivatives Catalyzed by AlCl3/H2SO4 under Heterogeneous and Mild Conditions, Chinese J. Catal. 29 (2008) 86–90. https://doi.org/10.1016/S1872-2067(08)60016-9.

[48] N. Hossein, N. Roozberh, Rapid, efficient and one pot synthesis of anthraquinone derivatives catalyzed by Lewis acid/methanesulfonic acid under heterogeneous conditions, Dye. Pigment. 81 (2009) 259–263. https://doi.org/10.1016/j.dyepig.2008.10.019.

[49] B.R. Madje, K.F. Shelk, S.B. Sapkal, G.K. Kakade, M.S. Shingare, An efficient one-pot synthesis of anthraquinone derivatives catalyzed by alum in aqueous media, Green Chem. Lett. Rev. . 3 (2010) 269–273. https://doi.org/10.1080/17518251003776877.

[50] N. Hossein, S.S. Brojerdi, Facile and Efficient One-Pot Synthesis of Anthraquinones from Benzene Derivatives Catalyzed by Silica Sulfuric Acid, Polycycl. Aromat. Compd. 34 (2014) 504–517. https://doi.org/10.1080/10406638.2014.910238.

[51] L. Chen, C. Ma, X. Li, L. Lin, S. Yang, G. Li, First principles design of anthraquinone derivatives in redox flow batteries, Int. J. Electrochem. Sci. 12 (2017) 10433–10446. https://doi.org/10.20964/2017.11.35.

[52] S. Er, C. Suh, M.P. Marshak, A. Aspuru-Guzik, Computational design of molecules for an all-quinone redox flow battery, Chem. Sci. 6 (2015) 885–893. https://doi.org/10.1039/c4sc03030c.

[53] R. Chen, Toward High-Voltage, Energy-Dense, and Durable Aqueous Organic Redox Flow Batteries: Role of the Supporting Electrolytes, ChemElectroChem. 6 (2019) 603–612. https://doi.org/10.1002/celc.201801505.

[54] Y. Hui, E.L.K. Chng, C.Y.L. Chng, H.L. Poh, R.D. Webster, Hydrogen-bonding interactions between water and the one- And two-electron-reduced forms of vitamin K1: Applying quinone electrochemistry to determine the moisture content of non-aqueous solvents, J. Am. Chem. Soc. 131 (2009) 1523–1534. https://doi.org/10.1021/ja8080428.

[55] C. Costentin, Update 1 of: Electrochemical approach to the mechanistic study of proton-coupled electron transfer, Chem. Rev. 110 (2010) PR1–PR40. https://doi.org/10.1021/cr068065t.

[56] M. Gómez, F.J. González, I. González, Intra and intermolecular hydrogen bonding effects in the

electrochemical reduction of α-phenolic-naphthoquinones, J. Electroanal. Chem. 578 (2005) 193–202. https://doi.org/10.1016/j.jelechem.2004.12.036.

[57] Y.A. Gandomi, D.S. Aaron, Z.B. Nolan, A. Ahmadi, M.M. Mench, Direct measurement of crossover and interfacial resistance of ion-exchange membranes in all-vanadium redox flow batteries, Membranes (Basel). 10 (2020) 126. https://doi.org/10.3390/membranes10060126.

[58] A. Lê, D. Floner, T. Roisnel, O. Cador, L. Chancelier, F. Geneste, Highly soluble Fe(III)-triethanolamine complex relevant for redox flow batteries, Electrochim. Acta. 301 (2019) 472–477. https://doi.org/10.1016/j.electacta.2019.02.017.

[59] Y. Jing, E. Wenbo Zhao, M.-A. Goulet, M. Bahari, E.M. Fell, S. Jin, A. Davoodi, E. Jónsson, M. Wu, C. Grey, R.G. Gordon, M.J. Aziz, Electrochemical Regeneration of Anthraquinones for Lifetime Extension in Flow Batteries, ChemRxiv. Cambridge Cambridge Open Engag. (2021). https://doi.org/10.33774/chemrxiv-2021-x05x1.

Supporting information

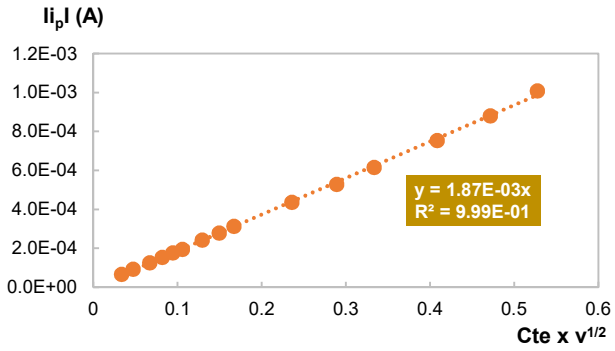

Figure S1 Diffusion coefficient evaluation of 2,3-DHAQ according to Randles-Sevcik method.

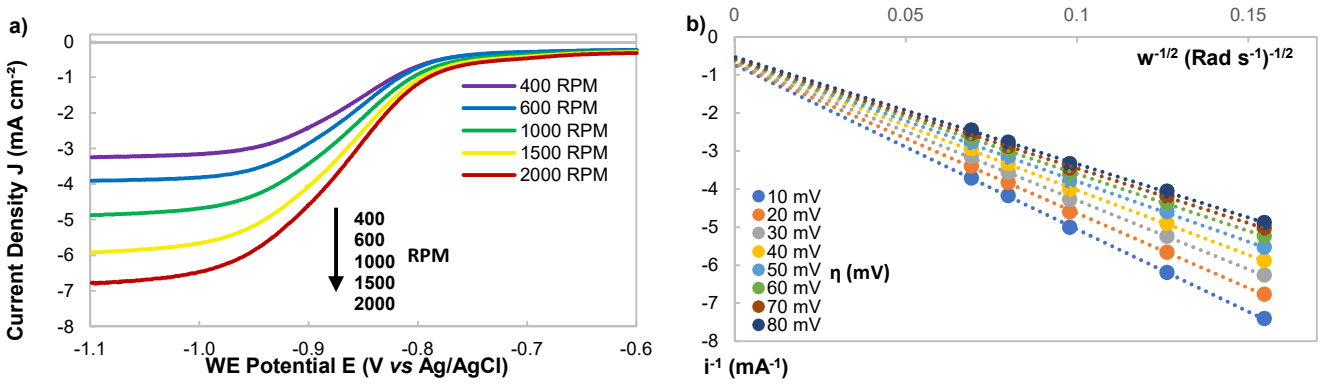

Figure S2 Determination of i_K according to Koutecký-Levich method.

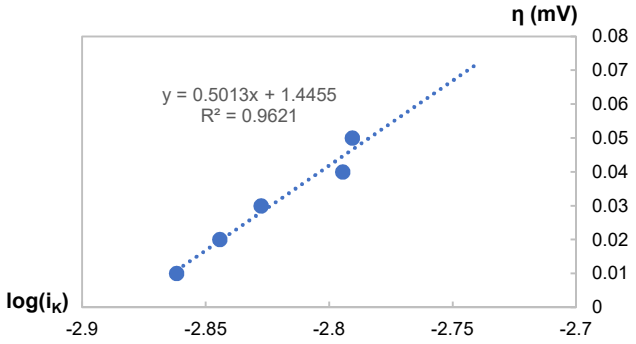

Figure S3 Determination of i_0 according to the Tafel equation.

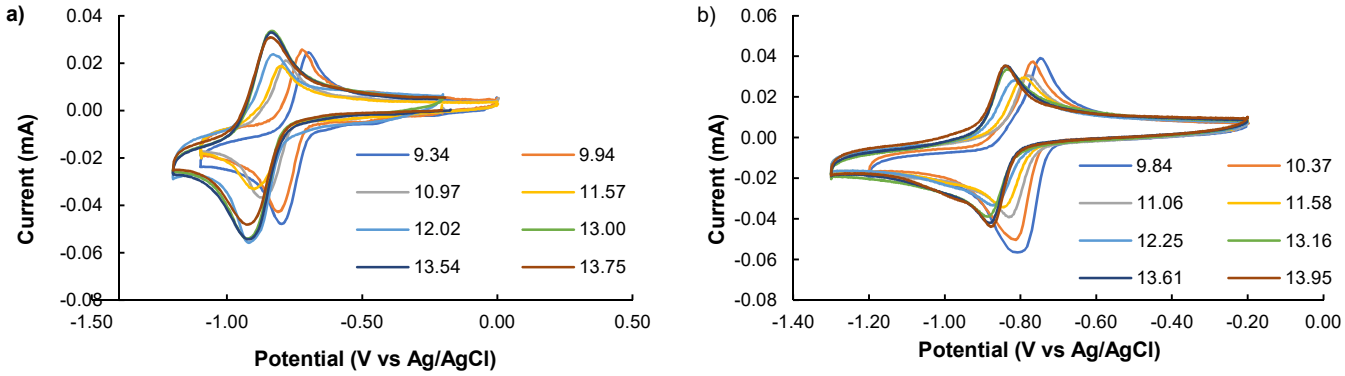

Figure S4 Cyclic voltammetry performed to determine Pourbaix diagram of a) 2,3-DHAQ and b) 1,2-DHAQ.

Electrochemical reversibility

Alan J. Bard *et al.* presented the five criteria defining the reversibility of a redox process in the handbook of electrochemical methods which are the following: i) the peak current absolute values must be proportional to the square root of the scan rate; ii) the peak potentials must be independent at all scan rates; iii) the potential peak difference must be equal to 59/n, n = number of electron involved in the redox process (2 electrons in this case); iv) the ratio of peak current absolute values must be equal to the unity; v) the apparent standard redox potential must be equal to the half-wave potential. Regarding 2,3-DHAQ, the compound fills most (4 over 5) of theoretical reversibility criteria (Figure S6 and Table 1 in SI).

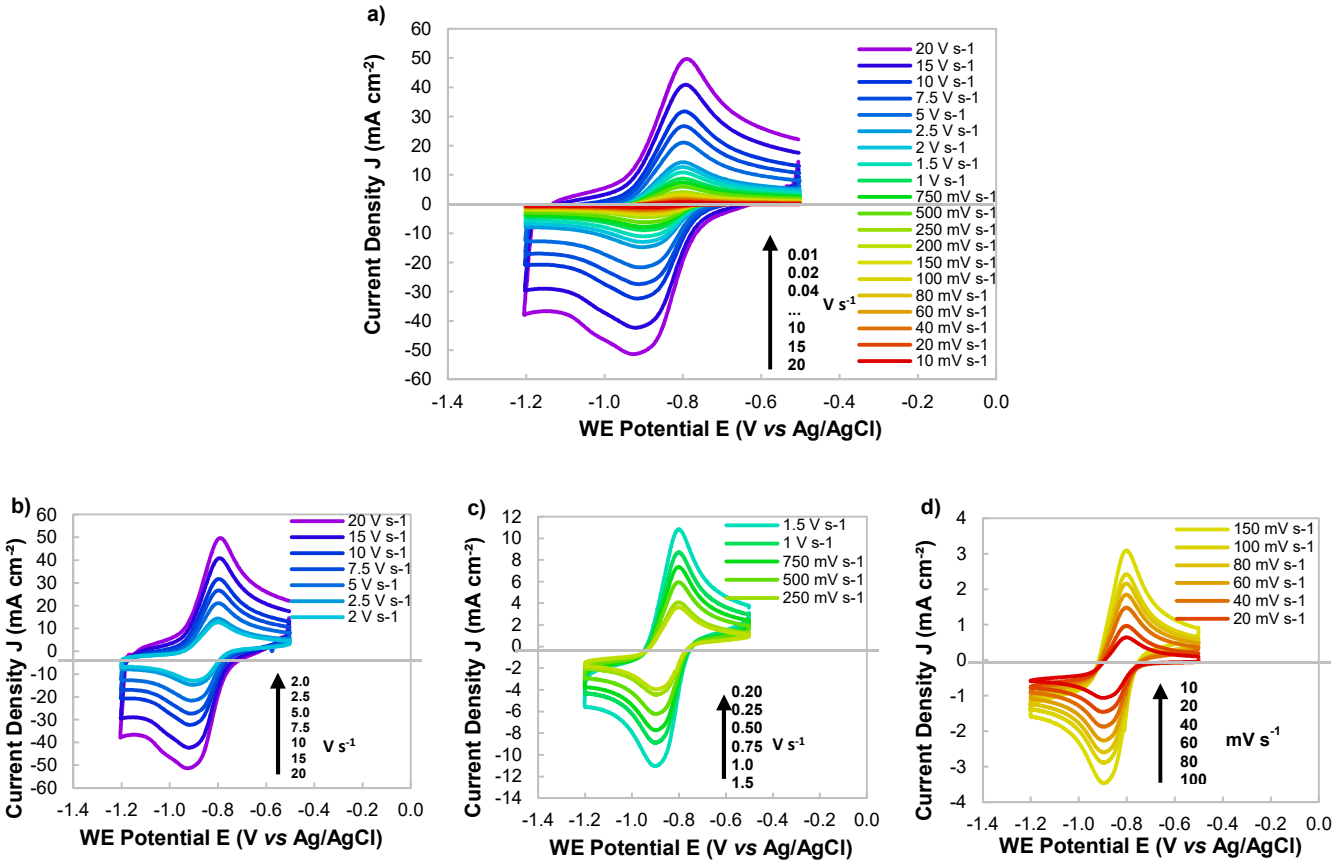

Figure S5 Cyclic voltammetry experiments of 2,3-DHAQ compound at a concentration of 6.3 mM in a KOH 1 M solution (pH 14). Several cycles were performed at faster scan rates (5 cycles from 20 down to 1.0 V s^{-1}; 4 cycles from 0.75 down to 0.20 V s^{-1}; 2 cycles from 0.15 down to 0.04 V s^{-1} and one cycle at 0.02 and 0.01 V s^{-1} scan rate) in order to stabilize the electrochemical signal and last cycles were plotted on 4 different graphs in order to give greater visibility of each redox response. In that respect, scan rates ranging from a) 20 down to 0.01 V s^{-1}; b) 20 down to 2.0 V s^{-1}; c) 1.5 down to 0.20 V s^{-1}; d) 0.15 down to 0.01 V s^{-1} were plotted.

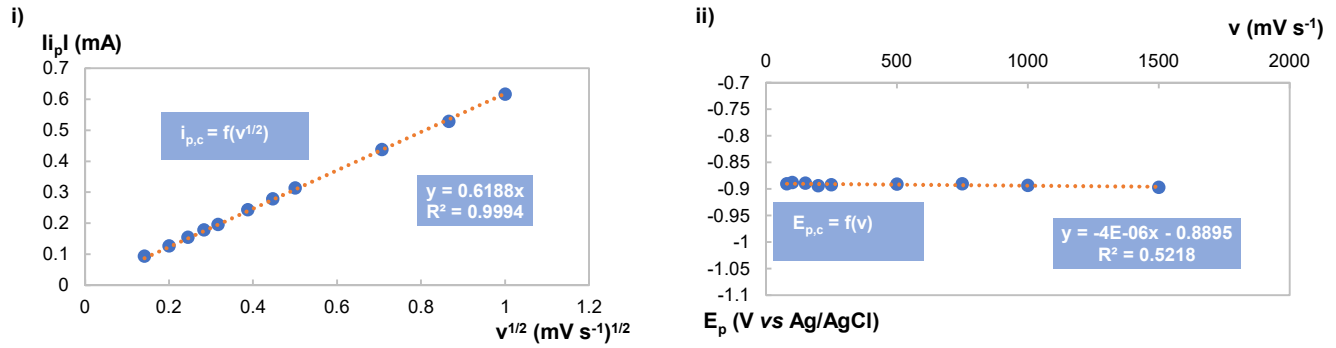

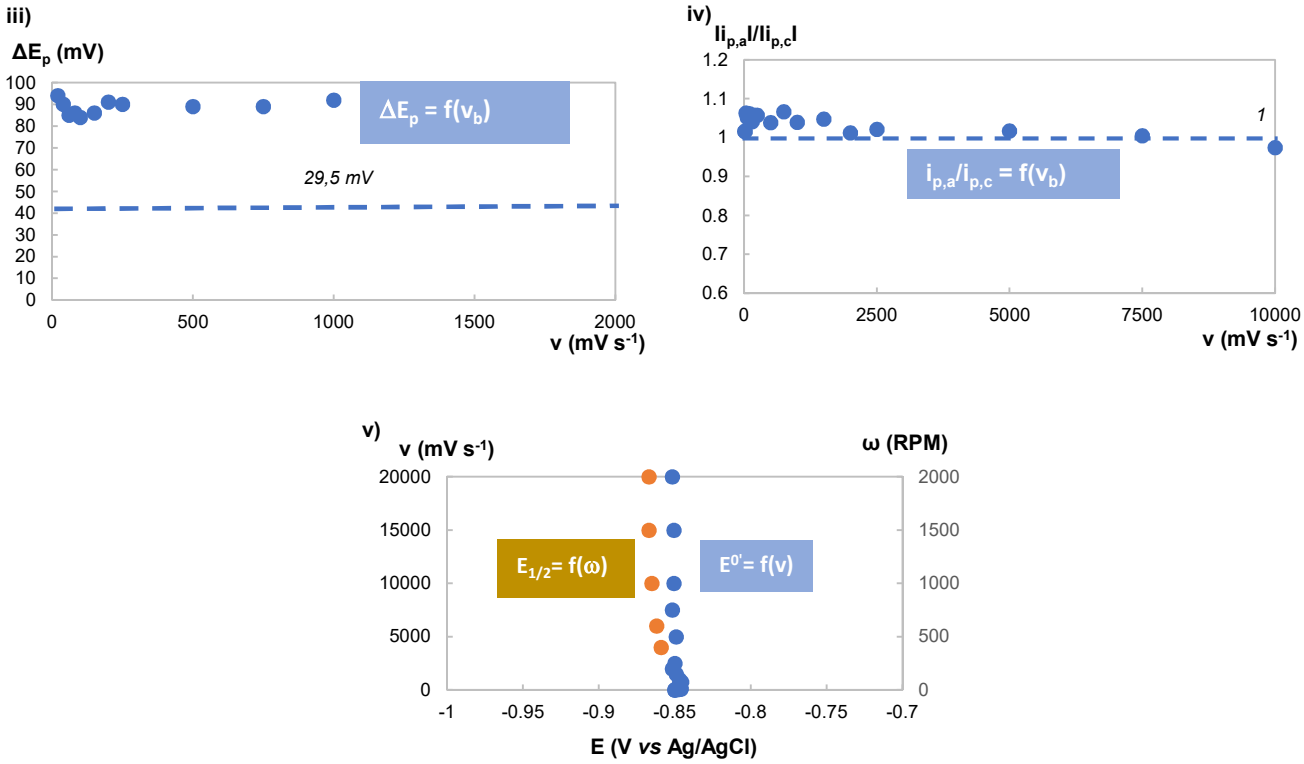

Figure S6 Reversibility criteria evaluation of compound 2,3-DHAQ.

Reversibility criteria	Evaluation	Interpretation	Result
i) $i_{p,c}$ α $v^{1/2}$	validated (99.99% correlation)	Reversible	**Reversible**
ii) $E_{p,c}$ independent from v	validated but slight deviation	Reversible	
iii) $\Delta E_p \approx 59/n$ mV	not validated (88 mV average)	Quasi-reversible	
iv) $i_{p,a}/i_{p,c}$ = 1 & independent from v_b	validated (1.04 average)	Reversible	
v) $E^{0'} \approx E_{1/2}$	validated (by < 15 mV)	Reversible	

Table S1 Reversibility criteria interpretation of 2,3-DHAQ compound.

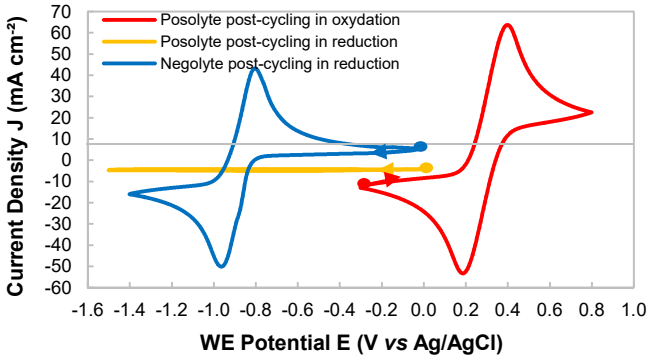

Figure S7 Voltammetry at 100 mV s^{-1} of post-cycling negolyte (blue) in reduction; post-cycling posolyte (red) in oxidation and (orange) in reduction.

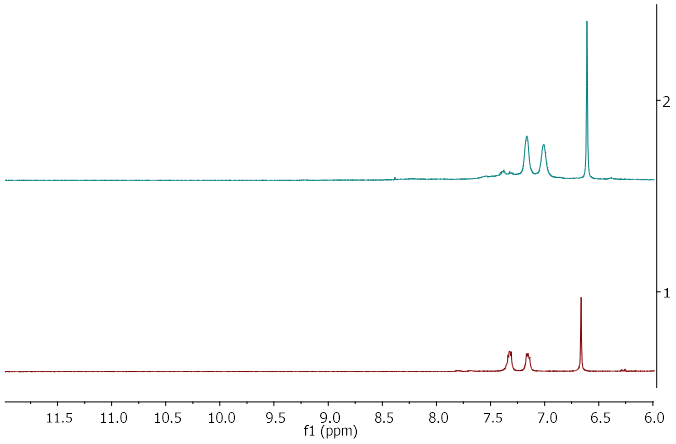

Figure S8 ^{1}H NMR of the negolyte before (red) and after (blue) 3000 cycles.